Sedimentary Geology

Precambrian fans on opposite margins of an intracratonic rift basin; palaeogeography, palaeoclimate and provenance: Neoproterozoic Badami Group, Karnataka, India

--Manuscript Draft--

Manuscript Number:	SEDGEO8484R1
Article Type:	Research Paper
Keywords:	Facies and Architectural Elements; CIA and Palaeoweathering trends; Provenance; Sequence Stratigraphy; Neoproterozoic Badami intracratonic rift basin; Rodinia breakup.
Corresponding Author:	Pradip Samanta, Ph.D. University of North Bengal Darjeeling, West Bengal INDIA
First Author:	Pradip Samanta, Ph.D.
Order of Authors:	Pradip Samanta, Ph.D.
	Soumik Mukhopadhyay, Ph.D.
	Arunava Sen, M.Sc.
	Nipun Ghosh, M.Sc.
	Adam Bumby, Ph.D.
Abstract:	An integrated approach of facies analysis, architectural element analysis and geochemistry provides significant insight into the palaeogeography, palaeoclimate and provenances of alluvial sediments in the Neoproterozoic Badami intracratonic rift basin, India. Process-based facies analysis identified twelve facies, grouped into five facies associations that record a palaeoenvironmental setting ranging from screecone – alluvial fan to braided fluvial. Rockfall and debris flow dominate the depositional processes in the screecone – proximal fan settings, whereas streamlet, sieve and sheetflood processes characterize the middle to distal fan palaeogeography. Furthermore, a distal braided fluvial system developed with decreasing depositional slope. Streams within the distal fan had ephemeral flow whereas the braided fluvial setting had semi-perennial to perennial flow. The braided fluvial basin expanded temporally; channels become shallower and wider in response to base profile rise and ultimately drowned under the sea. The poorly sorted clastic deposits of the studied interval are interpreted as a lowstand product. The water table primarily controls spatial variability in flow duration within channels. Nevertheless, temporal water table rise due to a change in climate resulted in persistent flow duration within the fluvial system. The screecone - alluvial fan setting developed on both margins of the east-west trending basin following northerly and southerly palaeoslope respectively. However, associated braided fluvial deposits indicate a westerly dipping palaeoslope, inferred from palaeocurrent directions, which corroborate an intracratonic rift setting. Major and trace element geochemistry and molar A-CN-K plots, CIA and palaeoweathering trends of sandy sediments traced ‘transitional/uplifted continental’, mixed provenances in the north, south and eastern parts of the basin ranging in age from Archaean to Mesoproterozoic. The rifting is inferred to be related to Rodinia supercontinent breakup.

Precambrian fans on opposite margins of an intracratonic rift basin; palaeogeography, palaeoclimate and provenance: Neoproterozoic Badami Group, Karnataka, India

Pradip Samanta[1]*, Soumik Mukhopadhyay[2], Arunava Sen[2], Nipun Ghosh[3] and Adam Bumby[4]

[1] Department of geology, University of North Bengal, Darjeeling, Siliguri – 734 013

[2]Department of Geological Sciences, Jadavpur University, Kolkata – 700 032

[3]Atomic Minerals Directorate for Exploration and Research, Bengaluru – 560 072

[4]Department of Geology, University of Pretoria, South Africa

*Corresponding author's e-mail: samanta.pradip@gmail.com/ geolps@nbu.ac.in

ABSTRACT

An integrated approach of facies analysis, architectural element analysis and geochemistry provides significant insight into the palaeogeography, palaeoclimate and provenances of alluvial sediments in the Neoproterozoic Badami intracratonic rift basin, India. Process-based facies analysis identified twelve facies, grouped into five facies associations that record a palaeoenvironmental setting ranging from screecone – alluvial fan to braided fluvial. Rockfall and debris flow dominate the depositional processes in the screecone – proximal fan settings, whereas streamlet, sieve and sheetflood processes characterize the middle to distal fan palaeogeography. Furthermore, a distal braided fluvial system developed with decreasing depositional slope. Streams within the distal fan had ephemeral flow whereas the braided fluvial setting had semi-perennial to perennial flow. The braided fluvial basin expanded temporally; channels become shallower and wider in response to base profile rise and

ultimately drowned under the sea. The poorly sorted clastic deposits of the studied interval are interpreted as a lowstand product. The water table primarily controls spatial variability in flow duration within channels. Nevertheless, temporal water table rise due to a change in climate resulted in persistent flow duration within the fluvial system. The screecone - alluvial fan setting developed on both margins of the east-west trending basin following northerly and southerly palaeoslope respectively. However, associated braided fluvial deposits indicate a westerly dipping palaeoslope, inferred from palaeocurrent directions, which corroborate an intracratonic rift setting. Major and trace element geochemistry and molar A-CN-K plots, CIA and palaeoweathering trends of sandy sediments traced 'transitional/uplifted continental', mixed provenances in the north, south and eastern parts of the basin ranging in age from Archaean to Mesoproterozoic. The rifting is inferred to be related to Rodinia supercontinent breakup.

Keywords: Facies and Architectural Elements; CIA and Palaeoweathering trends; Provenance; Sequence stratigraphy; Neoproterozoic Badami intracratonic rift basin; Rodinia breakup.

1. INTRODUCTION

The rudaceous sedimentary cone deposits are mostly formed in tectonically active margins, and consequently prone to disturbances, and eventual destruction. Therefore, reconstruction of such cones is often very difficult, particularly for those from the Precambrian. The general lack of vegetation during the Precambrian promoted formation of such sedimentary cones, as slopes were more vulnerable to failure, producing debris flows (Bose *et al*., 2008). Published records of the Precambrian screecone deposits are very rare. Nonetheless, the dominance of

early greenhouse gasses in the Precambrian atmosphere facilitates more rigorous palaeoweathering conditions and consequently produces more labile constituents in the flows. Greater availability of fines would have produced more hyperconcentrated mass flow products (Long, 2004) even within the fluvial systems (Buck and Minter, 1985). Therefore, differentiating alluvial fans from coarse grained fluvial deposits remains a challenge for Precambrian deposits (Miall, 1996; Els, 1998; Bridge, 2003; Eriksson *et al*., 2006). Lithology, facies, petrography and geochemistry of these clastic sediments provide ample important information about past tectonic (Bose *et al*., 2008) and climatic settings (Waters *et al*., 2010), as well as their provenances (Lamminen and Köykkä, 2010).

The detrital modes of sandstone can be used quantitatively, calculated from point counts of thin sections to infer the tectonic settings of provenances (Dickinson *et al.*, 1985). The mineralogical and bulk chemical compositions of sedimentary rocks are useful in determining provenance, interpreting palaeoclimates and tectonic activity (Nesbit *et al*., 1996). Hydraulic sorting, weathering and diagenesis has a strong influence on geochemical alteration of the source sediments. Nonetheless, the signature of the original source terrain often remains within the sediments, reflecting the nature of the exposed continental crust (Taylor and McLennan, 1985). The water-mobile major and trace elements, such as alkali and alkaline earth elements are very sensitive to climate change and can be used as an important proxy for depositional environments and palaeoclimate evolution (Wei *et al*., 2004). The introduction of discrimination diagrams based on the relationship of major and trace elements are now used to determine sediment provenances (Yan *et al.*, 2007).

This present study deals with the uraniferous screecone-alluvial fan and associated braided fluvial deposits at the base of the Neoproterozoic Badami Group. Belgaum, Karnataka, India. Spectacular preservation and exposures provide ample opportunity to examine the tectonic and climatic control, and source rock characteristics. The work has been

performed covering an area of about 3000 sq. km where breccia, conglomerate and poorly sorted sandstone bodies, unconformably overlie the basement rocks of the Mesoproterozoic Bagalkot Group and Archaean metasediments. Seven representative sections in five different localities, namely, Murgod, Deshnur, Gokak, Gujanal and Islampur are studied (Fig. 1). All the localities are in the western sector of the east-west trending Badami basin, covering the northern, western and southern margins of the basin (Fig. 1). The studied stratigraphic interval represents the basal members of the Badami Group, viz., Kendur Conglomerate Member overlain by the Cave Temple Arenite Member (Fig. 2). The palaeogeography of the above sectors of the basin can be determined separately by process-based facies analysis. Distribution of facies in time and space in conjugation with location-wise and facies-wise palaeocurrent analysis help in the understanding of the palaeodrainage pattern, indicating the general palaeoslope direction within the study area. This paper also examines the evolution of facies, fluvial architecture in order to assess the spatial and temporal variations in sedimentation patterns and their possible controlling factors. Petrographic and geochemical investigations were performed to investigate the sources or provenances of the sediments and also to infer the tectonic setting of the basin.

2. GEOLOGICAL AND TECTONIC SETTING

The Bagalkot and Badami groups together constitute the Kalagdi Supergroup, and are thought to have been deposited in a broadly east-west trending oval shaped episodically sinking intracratonic basin (Fig. 1; Kale and Phansalkar, 1991, Mukhopadhyay *et al*., 2019). The airborne geophysical and satellite data reveal that the basin is confined between basin margin fault systems and is also traversed by several E-W to NE-SW trending faults and lineaments (Fig. 1B; Sridhar *et al*., 2014). The lack of volcanics with the associated

sediments has been attributed to development up to pre-rift stage of the basin (Dey, 2015). A U-Pb baddeleyite age of a dolerite dyke intruding the Yendigere Formation limits the minimum age of deposition for the lower Bagalkot as 1861±4 Ma (Joy *et al.*, 2018). The 1154±4 Ma age by $^{40}Ar/^{39}Ar$ dating method of mafic dykes associated with the Mallapur intrusives that cut the uppermost Bagalkot Group, represents the post sedimentary igneous event, and indicates that the Badami sedimentation must have taken place after 1.1 Ga (Patil Pillai *et al.*, 2018). On the basis of U-Th-Pb and Rb-Sr radiometric dating of limestone and glauconitic sandstone of the Bhima Group and the Badami Group, Joy *et al*. (2018) suggested that these two basins are contemporary and ascertained the depositional age as 800-900 Ma. The Badami Group, unconformably overlies the middle Riphean Bagalkot Group and Archaean metasediments, is divided into Kerur and Katageri formations in ascending order that are, in turn, subdivided into six members (Jayaprakash *et al*., 1987; Fig. 2). The lower two members of the basal Kerur Formation are characterized by lenticular, poorly sorted sandstone and conglomerate bodies of largely fluvial origin (Hegde *et al*., 1994; Dey *et al*., 2009; Mukhopadhyay *et al*., 2014, 2019). The top two members outcrop sparsely, and are composed of fine grained clastic deposits relating to a marginal marine setting (Mukhopadhyay *et al*., 2014). The Kerur Formation gradually passes upward into the Katageri Formation, comprising shale-limestone of probable marine origin (Jayaprakash *et al*., 1987; Kale and Phansalkar, 1991). The Kerur Formation in the western sector, informally divided into four lithological units, has a lower conglomerate at the base, followed by lower arkose, upper conglomerate and an upper arkose unit at top (Fig. 2). The present study focuses on the lower conglomerate and the basal part of lower arkose unit outcropping in and around Belgaum district (Figs. 1, 2).

3. METHODS

This study was undertaken using field, petrography and geochemical data. 25 out of 28 fresh samples of sandstones, and conglomerates with sandy (and rare mud) matrix have been utilized for quantitative mode analysis (Dickinson and Suczek, 1979*;* Dickinson, 1985), These 25 samples represent different facies and facies associations (described later) at a variety of locations (Table 1). Modal point calculations were carried out, using a petrographic microscope, for 200 point counts at 3 different parts of the petrographic thin sections for each specimen from which average modal percentage of minerals were calculated (Table 2). Three of the 28 samples represent the matrix of debris flow conglomerates (sample no. 1, 20 and 21; Table 1), and have been excluded on account of their higher clay content (>20%). 15 from the 28 samples of sand-dominated bulks were selected for major and trace element studies. The samples were cut into thin (approximately 5 mm thick) slices along sections perpendicular to bedding, washed with distilled water and wiped with acetone to remove surficial contamination. These slices were powdered using a hand-driven agate mortar and pestle. The grinding and powdering were carried out manually using nitrile gloves. Major oxide concentrations (Table 3) of sample number 1, 2 and 12 to 15 (6 samples) were determined in pressed pellet form using the Rigaku ZSX Primus II wave length dispersive X-ray fluorescence spectrometer (WD-XRF) with a 4 kW Rh target, operated at 60 kV and 50 mA at the Indian Institute of Technology (IIT) Kanpur, India following the procedure described in Amir *et al*. (2018). Sample numbers 3 to 11 (9 samples) were analysed using the Wavelength Dispersive X-ray Fluorescence (WDXRF) S8 Tiger (4Kw) from Bruker-AXS, Germany at the Indian Institute of Science Education and Research (IISER) Kolkata, India following the procedure described in Das *et al.* (2020). Two standard reference materials, MESS-3 (Certified Reference Material, CRM) certified by National Research Council of Canada (NRC - CNRC) and USGS geochemical reference material SDC-1, were analysed with each

batch of unknown samples to determine the accuracy of analyses (Supplementary Table ST1). Loss of Ignition (LOI) of all the 15 samples was determined by igniting 1g of powdered sample in a Platinum crucible up to 1050°C for 4 hours at IIT Kanpur. No other samples except sample number 11 show visible phases of carbonates during petrographic investigations and consequently all the 14 other samples show very low values of LOI corresponding probably with the low contents of clay, phosphate and organic phases. For CaO* correction, weight percentage of CO_2 was measured analytically only for sample number 11 (Table 3). The loss of CO_2 was determined by adding 1g to 5g of powdered sample number 11 to warm 0.1 N HCl following a semi quantitative gravimetric method. 200 ml of warm HCl was, poured in a 250 beaker, placed on analytical balance and tarred. Powered samples (1g to 5g respectively) were weighed accurately and were added to acid and the weight changes were recorded until completion of the effervescence reaction (supplementary Table ST2). The amount of carbon dioxide released followed a linear regression relationship with the initial weight of the sample (regression coefficient R^2 value of 0.9983, supplementary Fig. SF1). Average weight percentages of released CO_2 were calculated from the mentioned trials. CaO* were determined for all the samples and corrected for phosphate phases (McLenan, 1993), however, for sample number 11 it was corrected for both phosphate and carbonate phases (Fedo *et al*., 1995).

Trace element concentration of 15 samples were performed at IIT Kanpur (Table 3) using the Thermo Fisher Scientific, 8900-Q-ICP-MS (Quadrupole Inductively Coupled Plasma Mass Spectrometer), both in standard and He Kinetic Energy Discrimination mode to optimize the separation of measured elements from interfering polyatomic interferences. Approximately 0.25g powdered sample was digested by a mixture of trace element grade HF and HNO_3 in 3:1 ratio using a pre-cleaned Teflon beaker at 130 ± 5^0C for 48 hours. After digestion, the samples were dried and re-dissolved in concentrated 2ml of Aqua-regia. If

residues were seen, the steps were repeated to complete the digestion process. Trace element concentrations were determined at ~200 ppm totally dissolved solid solutions. Reference Materials SBC-1 and SCO-1 (shale) from the US Geological Survey (USGS) and WGB-1 (Gabbro) rock standard from Canadian Certified Reference Material Project (CCRMP) were also digested following the same procedures (supplementary Table ST3). Three blanks were analysed to quantify the total procedural blank, whereas reference materials were analysed as unknown to assess the data quality. Multi elemental standard solution (MES) diluted to 7 appropriate concentrations was used to construct the calibration curve, and trace element concentrations were determined based on the calibration curve. Since exact rock-matrix matched reference materials were unavailable, all the samples and standards were spiked by ~5 ppb rhodium solution, and rhodium was used as an internal standard. Average blank corrections were less than 1% for most of the elements.

4. FACIES ANALYSIS

Facies have been classified on the basis of sedimentary structures, body geometry and textural characteristics. A unified facies analysis scheme is adopted based on depositional mechanism of the sediments (Walker 1984; Reading 1986; Posamentier and Walker 2006). Twelve (12) facies have been identified, the details of which are given in Table 4.

5. FACIES ASSOCIATIONS

Facies can be grouped into several genetic packages, called facies associations (FA) (Miall, 1980; Hallam, 1981; Walker, 1984; Reading, 1986). A particular facies association differs from others in overall combination of facies, their mutual proportions, internal organization

and body geometries, although a particular facies can be shared by different associations. Five distinct facies associations can be ascertained for the entire studied interval (details given in Table 5). FA 1 composed of breccia and conglomerate facies representing screecone palaeogeography. FA 2 composed of coarsening upward succession of conglomerate with subordinate sandstone and breccia facies representing an alluvial fan. FA 3, 4 and 5 composed dominantly of sandstone facies representing braided fluvial setting, however, deposited in ephemeral, semiperennial and perennial flow condition respectively.

6. FLUVIAL ARCHITECTURAL ELEMENTS

Fluvial architectural element analysis is instrumental for understanding the palaeogeomorphology and fluvial channel patterns of any fluvial deposit. The architectural elements are identified on the basis of lithology, internal structure and 3-dimensional geometry of the macroforms that are larger than bedforms but smaller than channels (Miall, 1985, 2006; Yu *et al*., 2002; Miall and Jones, 2003; Fielding, 2006; Sarkar *et al*., 2012). The constituents of the architectural elements of the fluvial deposits have been given in Table 6.

7. FLUVIAL BOUNDING SURFACES AND PACKAGING PATTERNS

Recent studies on fluvial sedimentology extend the premise of architectural element analysis by recognising strata-bounding surfaces (Miall, 1985, 1988, 1992, 1994, 1996, 2006; Bromley, 1991; Eberth and Miall, 1991; Fielding, 1993; Hjellbakk, 1997; Yu *et al*., 2002; Bridge, 1993, 2006; Miall and Jones, 2003; Best *et al*., 2003; Gani and Alam, 2004; Alexander and Fielding, 2006; Catuneanu, 2006; Long, 2006; Rygel and Gibling, 2006; Gao *et al*., 2007). The larger surfaces discriminate elements larger than channelforms, like channel

belt cycles and valley cycles (Miall, 1988; Holbrook, 2001; Catuneanu, 2006). Comparatively smaller surfaces characterize the stratal packaging types within such channel belts or valley fills. The packaging pattern in FA 3 is characterized by the lateral and vertical stacking of SCE without any major erosion surfaces (stratigraphic package, SP, 1). However, FA 4 and 5 are characterized by packaging of multiple vertical and laterally juxtaposed architectural elements divided by laterally persistent master erosion surfaces that can be correlated with 'channel belts' of Holbrook (2001). In FA 4, each of the packages, stacked one above another, are broadly lenticular to tabular in geometry, separated by undulatory, incised bounding surfaces (stratigraphic package, SP, 2). FA 5, on the other hand, is composed of packaging of sheet like sandstone bodies, with less scouring at the bounding surfaces (stratigraphic package, SP, 3).

The general absence of master erosion surfaces in SP 1 possibly reflects frequent incision by small channel elements and their occurrence too close to each other (Fig. 4E). This package pattern suggests formation of interconnected networks of channels in a braided pattern, where omission surfaces are often eroded, indicating frequent abandonment and reoccupation of channels. Local occurrences of soft sediment deformation structures (Fig. 7H) and the presence of massive to crudely cross stratified flash flood deposits with randomly distributed oversized clasts clearly suggest highly the fluctuating nature of the flows within ephemeral channels (Olsen, 1989). In SP 2, each storey comprises rows of three to four architectural elements, viz. DAE, SCE, LSE and minor LAE stacked one above the other, with rare SGE. DAE and SCE, both rest on the bounding surface, and are laterally adjacent and transitional to each other. The LSE frequently underlies bounding surfaces and generally overlies DAE and LAE. Frequent lateral transitions between DAEs and SCEs or LAEs apparently attest to the mid-channel position of the bars, which likely formed in a braided river system (Miall, 1996; Sarkar *et al.*, 2012; Samanta *et al.*, 2016). Scouring (<15 cm)

within SP 2 reflects that flow unsteadiness still existed, although to a lesser extent. The river channels were probably semi-perennial in nature. SP 3 is comprises mostly DAE, TBE, SCE and LAE. The bar-top planar laminae with limited grain size variations between various elements suggest the limited scale of flow fluctuation during filling of the channels. The bounding surfaces, separating each package, are more planar and the lack of significant scouring at their bases clearly suggests more stable flows in a braided pattern of river system, like SP2. The occurrence of transverse bars within this package supports declining flow velocity within the channels. Therefore, it can be inferred that the channels become increasingly perennial distally. Nonetheless, the drainage basin expanded by denudation and headward erosion of higher topographic areas during deposition of SP 2 and 3. Over time, these two fluvial intervals covered all the study area, eventually overlying all other stratigraphic units (except FA 1), even onlapping the basement (Fig. 12).

8. STRATIGRAPHIC ARCHITECTURE

The stratigraphic architecture in all locations is based on the visual appreciation of lateral and vertical transitions depending on the exposures. In most of the areas, construction of synthetic vertical sections along the dip direction, has been undertaken, except Murgod, where vertical sections are constructed at three different locations (Fig. 1C), each successively further away from the basin margin accordingly named as ‘proximal’, ‘middle’ and ‘distal’.

The **Proximal** section, in the Murgod area, is composed almost entirely of FA 1 (Fig. 8), directly overlying the metasedimentary Saundatti Quartzite basement, and representing the only outcrop (Location S-1, Fig. 1B and C) of this association. The scree breccia facies dominate in this section and these are thicker and coarser than other constituent facies, although rapidly wedge downslope. The clasts composition of the breccia and conglomerates

are almost entirely made up of quartzites (Fig. 8). The palaeocurrent direction derived from the fan apron subfacies shows considerable variations, although very few data are available. The **Middle** section is around 200 m downcurrent from the proximal section (Location S-2, Fig. 1B and C) and overlies it. This section is comprised mostly of pebbly sandstone bodies (FA 3) with infrequent debris flow conglomerates (facies B) towards the basal part (Fig. 8). The debris-flow conglomerates are progressively reduced in frequency up the section with a gradual increase in channel width. The maximum channel width in the lower part measured up to 2.3 m whereas its average width is measured to be 4.5 m towards top. Grain flow conglomerate bodies (facies C), frequently associated with debris-flow in the proximal section, is absent within this section. Overall reduction in grain size of the sandstone bodies as well as thicknesses of the trough sets are apparent up-the-section. The **Distal** section is situated about 80 m away from the middle section along the depositional dip direction (Location S-3, Fig. 1B and C), and overlies it. This section is dominantly composed of FA 4 (Fig. 8). The facies constituents are pebbly, yet smaller in grain size than those of the proximal and middle section. However, the basal segment shows infrequent occurrences of trough cross stratified, pebbly sandstone bodies belonging to FA 3. The palaeocurrent direction of FA 4 shows an angular relationship to that of the FA 3 but is fairly consistent all through the basin (Fig. 8). This section also shows an upward decrease in grain size as well as set thicknesses.

The **proximal** section of the Murgod area suggests a screecone deposit. The high angularity of the clasts indicate proximal terrestrial palaeogeography, nearest to the basin margin. The **middle** section, dominated by trough cross stratified granular sandstone bodies of FA 3, suggests their deposition through a network of small, short-lived, highly avulsive, high energy streamlets. The palaeoslope appears to be too steep for the development of stable channelforms. Deposition apparently took place along less steep marginal areas of the

screecone. The dominance of FA 4 in the **distal** section suggests deposition from a comparatively stable braided semi-perennial river system. However, decrease in grainsize and cross set thickness up the section indicates rapid filling up of the site with reduction in slope and flow velocity, possibly at the fringe of the screecone. Evidently, FA 3 follows a different palaeoslope (north to north-west) than that of FA 4 (westerly) (Fig. 8).

The single measured section in the Gokak area, of about 17 m (Figs. 1, 9) is constructed along the deep gorge of the Gokak waterfalls (Location S-5, Fig. 1B). The succession, initiates with conglomeratic FA 2, overlies granitic basement (Fig. 9), and is followed upward by sandy deposits of FA 5 (Fig. 10). FA 2 shows a prominent coarsening-upward trend, with a sandy lower portion (Fig. 10). Occasional sheet flow and debris flow conglomerate bodies are dispersed within the lower sandy portion. The middle portion is dominated by sheet flow conglomerates and sieve deposits, whereas the upper portion is dominated by debris flow conglomerates. Rare scree breccia bodies are found to be dispersed at different levels of the association (Fig. 10). Conglomerate bodies thickened and coarsened upward, amalgamations of which are more common towards upper portion than the middle portion (Fig. 9). The clasts of these breccia and conglomerates are mostly granitic but BIF and other clasts constitute a significant proportion of the sediment budget (Fig. 9). This conglomeratic interval is succeeded by pebble-free sandy fluvial deposits of FA 5, with a sharp contact (Figs. 9, 10). This association, with its typical multistoried appearance, makes up the majority of the total succession and showing a fining upward trend. A few laterally extensive soft sediment deformation layers are also encountered in the basal portion of FA 5 (Fig. 9). The palaeocurrent directions derived from FA 2 shows an angular relationship with that of FA 5 (Fig. 9).

The basal conglomeratic portion of the succession, with its coarsening upward trend, undoubtedly represents a prograding alluvial fan (Middleton and Hampton, 1973, 1976;

Lowe, 1979; Nemec and Steel, 1984; Blair and McPherson, 1994). The lowermost sandy part with occasional sheet flow and debris flow conglomerates clearly suggests lower fan palaeogeography. The sheet flow and sieve dominated middle part and debris flow dominated upper part account for middle and upper fan palaeogeography, respectively. The occurrence of scree breccia bodies at different levels of the succession indicates tectonic upliftment of the basement thereby promoting prolonged progradation of the alluvial fan. The subsequent fluvial interval represents deposition from a braided perennial river system, onlapping over a gently sloping area beyond the basin marginal influence. The presence of laterally extensive soft sediment deformation structures within basal part corroborates tectonic disturbance (Allen, 1968). The angular relationship of palaeocurrents between FA 2 and 5 indicates that the short lived ephemeral river and alluvial fan systems developed along the local palaeoslope (southerly), whereas the perennial river system (FA 5) follows the regional westerly palaeoslope direction (Fig. 9).

In the **Deshnur** area (Location S-4, Fig. 1B), the succession is chiefly arenaceous with a thin basal rudaceous portion, overlying the Archaean metasediments (Fig. 11). The rudaceous portion is composed of intercalations between debris flow (facies B) and sheet flow (facies E) conglomerates and trough cross-stratified sandstone bodies (subfacies H_1), with rare occurrences of sieve (facies D), modified grain flow (facies C) and scree breccia (facies A) bodies. The overlying sandy portion consists of multistoried, several vertically juxtaposed channel belts of FA 4 and 5 successively with a distinct fining upward trend. The cross strata orientations for both the facies associations are fairly similar and consistent (Fig. 11).

The dominance of debris flow, sheet conglomerates and rare presence of sieve deposits in the basal portion suggest an alluvial fan palaeoenvironment (Wasson, 1974). Although a typical coarsening upward succession is absent (Rust and Koster, 1984; Nilsen,

1985; Blair and McPherson, 1994), representing the distal fringe of the fan. The frequent presence of channel thalweg conglomerates and overall very coarse grain-size indicate high energy deposition, probably on steep slopes. The overlying sandy facies associations with well-developed channel belt and channel fill bodies illustrate their deposition from a braided fluvial system in areas beyond the alluvial fan. The overall fining upwards trend within FA 4 and 5 clearly suggest aggradation with steady rise in base level.

The successions in the **Gujanal** and **Islumpur** localities (Location S-6 and S7, Fig. 1B) are chiefly arenaceous with dominance of trough cross stratified sandstone bodies (Fig. 12A). Both the successions are similar and are dominated by multistoried FA 4 and 5. Basement is not exposed, although granitic basement outcrops at a nearby locality (Fig. 12B). The rudaceous facies are almost absent except for the occurrence of a few channel thalweg conglomerates (facies F). A few laterally extensive soft sediment deformation layers are encountered within FA 5 in both localities (Fig. 12A).

The palaeogeography of FA 4 and 5 is similar to that of other areas with a similar regional palaeoslope as indicated by the consistent palaeoflow direction (Fig. 12).

9. PROVENANCE FROM SANDSTONE COMPOSITION

Modal proportions of mineralogical components of the 25 selected sandy specimens have been plotted in Q_t-F-L triangular plot (Dickinson, 1985; Fig. 13A) to help determine the provenance characteristics and tectonic setting. Most of the samples fall either in the field of 'transitional continent' or in the 'basement uplift' portions of the triangular diagram (Dickinson *et al*., 1983; Dickinson, 1985). Basement uplifts occur along incipient rift belts, transform ruptures, deep-seated thrusts, and zones of wrench tectonism. The foreland basin

model is not applied for the Badami as it is not associated with any middle Proterozoic mobile belt nor has any tectonized contact (Kale 1995). The Q_t-F-L triangular plot corroborates a intracratonic rift model for the Badami basin with transitional/uplifted continental source (Dey, 2015) leading to feldspar enrichment and preservation due to quick burial during the initial rift stage.

10. PALAEOWEATHERING TRENDS AND PROVENENCES

For comparison, all the data (Table 3) are normalized with the average Proterozoic Cratonic Sandstone (PCS; Condie, 1993) and average Upper Continental Crust (UCC; Taylor and McLennan, 1985; Rudnick and Gao, 2003) and are plotted in Fig. 13B and C, respectively. Compared to the PCS, the average trend for all the 14 samples (excluding sample number 11) show lower values of MgO, CaO and TiO_2, similar values of SiO_2, higher values of Na_2O and K_2O and slightly higher values Al_2O_3 and FeO_T. On the other hand, compared to the UCC the average compositional trend of the 14 samples shows slightly lower to similar values of K_2O, similar values of SiO_2, lower values of MgO, Na_2O, FeO_T, P_2O_5, TiO_2 and MnO and very low values of CaO. Major oxide data have been compared to the data from surrounding immediate basement rocks, like the Mesoproterozoic Saundatti Quartzite from the northern and southern basin margins (Dey *et al*., 2009), Archaean Peninsular Gneisses (PGC) (Dey et al., 2009), greywacke and phyllites from the Archaean Chitradurga and Gadag Schist belts (Naqvi *et al*., 1988), cherts, shales and BIFs from Chitradurga Schist Belt (CSB) (Rao and Naqvi, 1995), Chitradurga pillow basalts (Duraiswami *et al*., 2013), Closepet Granite (CG, Dey *et al*., 2009) and basalts of the late-Archaean Hungund-Kushtagi schist belt (Naqvi *et al*., 2006; Dey *et al*., 2009), to understand the sediment contribution from different aged rocks. A restricted cluster of data points can be seen within the total alkali contents ($K_2O + Na_2O$) vs.

K_2O/Na_2O diagram (Fig. 13D) and the data are closely associated with the northern Saundatti Quartzite and shales, shaly BIFs and phyllites of the Chitradurga metasediments. Total alkali content varies from 2.25% to 6.99% indicating variable feldspar content in sand-sized fractions along with variable clay content in the finer fraction. The K_2O/Na_2O ratio is always greater than 1 (max. 10.11 and min. 1.29; mean= 4.74) indicating predominance of K-feldspar. The SiO_2/Al_2O_3 vs $(FeO_T + MgO)/(K_2O + Na_2O)$ diagram (Fig. 14A) also shows data points for the samples clustering near the Saundatti specimens. A minimum value (3.66) of SiO_2/Al_2O_3 is demonstrated by clay rich sample 11, where most of the sand-sized samples have higher values, always above 10, with an average of 15.03. On the other hand, average $(FeO_T + MgO)/(K_2O + Na_2O)$ is 0.99 for 9 samples showing a value below 1. This indicates a greater contribution of clastic components from felsic, quartzo-feldspathic source than mafic and also a lesser clay content for the sand-sized fraction that corroborates petrographic observations. The enrichment of total iron oxide content (FeO_T), in contrast to overall lower values of CaO, TiO_2 and MgO, suggests a source that is rich in iron but devoid of other mafic components, like iron formations. Sample 11 contains calcitic cement, which explains the exceptional enrichment of CaO. The greater amount (24-26%) of fine-grained illitic and chloritic clay content is better reflected by the enrichment of K_2O, Al_2O_3, MgO and FeO_T and lower values of SiO_2. The higher values of MgO, FeO_T and TiO_2 suggest some contribution from mafic sources for the proximal rudaceous sediments, especially for products of debris flows, which may carry sediments from a long distance. The low $(FeOT+MgO)/(K_2O+Na_2O)$ values (average. 0.999) and high SiO_2/Al_2O_3 values (average. 15.028) (Table 5; Fig. 14A) reflect greater contribution from more evolved felsic or quartzo-feldspathic sources. SiO_2/Al_2O_3 values tend to reflect maturation of sediments, but without formation of excess clay due to greater chemical weathering rate and feldspar alteration. K_2O/Na_2O vs. K_2O+Na_2O plots (Figs. 13D) indicate major sediment contribution from an evolved K-rich

source, like Closepet Granite (K-rich granitoids) or Saundatti Quartzite (K-rich metasediments). Normalization with respect to UCC (Fig 13C) again indicates a felsic, potassium rich source rock with lesser contribution from iron rich and mafic sources.

Trace element data are plotted as Zr/Ni vs. Zr/Cr and Cr vs Ni diagrams (Figs. 14B, C) and they also have been compared to immediate basement rocks mentioned earlier. The data points in the Zr/Ni vs. Zr/Cr diagram (Fig. 14B) coincide with the granitoids and extend towards higher values. Samples show similar to slightly higher values than the Saundatti Quarzite from the southern margin, though are very similar to values from northern margin. The Chitradurga and Gadag phyllites and greywackes, shales, shaly BIFs and a few pillow basalts from the Chitradurga Schist Belt show closer association with the Badami sediments. In the Cr *vs* Ni diagram (Fig. 14C), the values are similar to those of the Saundatti Quartzite, show affinity to granitoid plutons and extend towards much lower values indicating greater contributions from granitoids and reworked quartzo-feldspathic Saundatti Quartzite, with some contribution from other sources like reworked metasediments of the Chitradurga Group.

Determination of Chemical Index of Alteration (CIA) values and plotting of an A-CN-K diagram (Nesbitt and Young, 1984, 1989; Nesbitt *et al*., 1996) reveal significant information about source contribution, patterns of palaeo-weathering, chemical evolution and alteration of sediments and climatic influences on the processes. Although the range of CIA (Table 3) varies from low to moderate values (48.14-65.74), the samples show an overall increasing trend of CIA values from FA 2 and 3 (48-55) to overlying FA 4 and 5 (56-66), with variable values for FA 1. In the molar Al_2O_3–(CaO + Na_2O)–K_2O or A–CN–K triangular plot (Fig. 14D), the studied samples show closer correlation with the Saundatti Quartzite and the K-rich Closepet granite. Here, the studied specimens plot along the direct weathering trend of K-rich Saundatti Quartzite and K-rich Closepet granite. The plotted data do not follow the direct weathering trend of the Peninsular granitoids or the schist belt

mafics. Low CIA values for FA 1, 2 and 3 (Fig. 14D) depict low rates of chemical weathering in a dry climatic condition. The relatively higher CIA values for FA 4 and 5 undoubtedly represent greater degree of chemical weathering resulting in greater loss of $CaO+Na_2O$ and K_2O and enrichment of Al_2O_3 in relatively wet and hot climatic condition (Yan *et al*., 2007). However, the exceptionally high CIA value for sample 11 is possibly not due to chemical alteration but corresponds to its primary matrix-supported mineralogy. The high CIA values within FA 4 and 5 may also be attributed to long transportation that accords well with the sedimentological observation, facilitating more pronounced chemical weathering during transportation.

11. DISCUSSION

Seven measured sections of the studied interval well-illustrate the lateral and vertical changes in the nature and organization of sediments during the early phase of development of the basin. The role of bedrock composition is apparent from the fact that metasedimentary basement generated steepest slopes while granitic basements gave rise to relatively gentle slopes on opposite sides of the basin margin. Most of the clasts are generally rectangular or blocky at Murgod area because of a closely jointed and well laminated metasedimentary source that contributed most of the sediments for the scree deposits. The rate of sediment supply must have been higher from metasedimentary sources as the sediments would have been weathered more rapidly. In general, the greater rate of sediment supply would have generated gentler slope and should have encouraged more sediment gravity flow products (Nichols and Thompson, 2005). However, despite the high sediment supply, Murgod area contains relatively few sediment gravity flow products, possibly because of the fact that the slopes in the area were steeper than the angle-of-repose for a considerable period of time, due

to syndepositional tectonic activity. This scenario likely resulted the accumulation of a considerable amount of scree deposits at the base of the Badami Group (cf. Bose *et al*., 2008). The Murgod area, therefore, represents the steepest southern margin of the study area, where the sedimentary cone deposits are coarsest and indicate sedimentation through free fall processes. However, the middle and distal sections of this area contain a subordinate amount of scree deposits and rapidly grade into SP 3 with a short intervention of SP 1 and 2, indicating the steepness of the basin margin. In contrast, the comparatively gentler slope in the Gokak area, representing the northern margin, facilitated more sediment gravity flows and consequently produced alluvial fans. The high rate of sediment supply relating to rapid uplift of the source area resulted in initial progradation of the alluvial fan. At Gokak, the massflow dominated alluvial fan deposit gives way upward into inferred SP 3 with a minor progradation at the basal part. It clearly suggests existence of slope break but the slope never appears to exceed the angle-of-repose. Occurrences of scree bodies well above the base of the succession suggest periodic upliftment of the basement. The presence of laterally extensive soft sediment deformation structures also corroborates tectonic disturbances (Allen, 1968). The tectonic activity was possibly not as frequent as at Murgod. The Deshnur area represents only the distal fringe of the inferred fan with dominance of SP 2 and 3. The channel belts become wider and thinner, at least in the distal part of this area, indicating even gentler slopes than those of Gokak. The Gujanal and Islampur aeras represent only SP 2 and 3 without preservation of any fan sediments, suggesting the gentlest slope of all the depositional sites.

The flow duration within channels, in its upstream reaches, depends on the availability of water sources and the position of channels with respect to the groundwater table. The topography, primarily controlled by tectonics, can also play a pivotal role in determining the position of water table with respect to the channel. In the downstream reaches sea level fluctuations play a significant role in controlling the channel parameters

(Blum and Tornqvist, 2000). The deceptive spatial variability in flow duration in the basinward direction, from either margin, within the studied interval was possibly controlled by seasonal variation in water table position with respect to the channels (Fig. 15). The control of water table fluctuation becomes far more important in the backdrop of dry, semi-arid to arid climatic conditions, with heavy seasonal rainfall, in combination with depauperated, primeval vegetation. In steeply sloping and higher topographic areas, like alluvial fan surfaces, water usually percolates downward rapidly from the channels, as the water table remains well below the channels for most of the year, except the times of rare heavy rainfall. In a multichannel system like SP 1, more deeply incised channels are likely to consume most of the water, leaving the shallower channels dry. Hence, an ephemeral nature becomes apparent. With decreasing steepness, the water table gradually rises to the channel surface resulting in semi-perennial nature of the SP 2 channels. With further decrease in steepness, the water table lies above the channel floor for most of the time of the year, and consequently accounts for the perennial nature of the SP 3 channels. Bose *et al.* (2008) reported a similar basin margin screecone-alluvial fan deposits from the underlying Bagalkot Group. They emphasised the flow durations down the hill slope and adjacent plains can solely be controlled by the position of the channels with respect to the groundwater intersection point, without necessitating any major change in climatic conditions.

However, the CIA values and weathering trends (Fig. 14D) clearly indicate that degree of chemical weathering increased during deposition of SP 2 and 3 compared to FA 1, 2 and SP 1. The low CIA values depicting weak chemical weathering, accord well with the overall arid to semi-arid climatic conditions during their deposition. The CIA plots of specimens from overlying SP 2 and 3 indicating comparatively higher degree of chemical weathering. Petrographic observations suggest comparatively higher amount of altered feldspar grains (Fig. 7E, F) within the sandstones, which supports this contention. The

shifting of values towards the K- apex are related to the incorporation Saundatti Quartzite as primary source that shows greater amount of K-feldspar due to both the effect of sediment sorting and minor redistribution of K due to K-metasomatism (Dey *et al*., 2009). Temporal expansion of the drainage basin within SP 2 and 3 suggests an elevation of the regional groundwater table throughout the study area, indicative of a climatic shift towards more wet and hot conditions. The divergent and location-specific palaeocurrent directions within FA 1, 2 and SP 1 clearly suggest that the scree breccia - alluvial fan and inferred ephemeral river systems were generated from the east-west trending basin margin fault systems and follow the extant slopes (northward at Murgod and southward at Gokak respectively) on either side of the basin margin (Fig. 15). However, consistent palaeocurrent directions within SP 2 and 3 indicate that the inferred semi-perennial to perennial river systems developed on plains likely represent the axial river that followed the regional westward palaeoslope (Fig. 15). The inferred depositional model (Fig. 15) clearly supports an intracratonic rift model for the Badami basin. The Qt-F-L triangular plot (Fig. 13A) further supports upliftment of the basement and quick burial of sediments, probably reflecting initial rifting stage of the basin. The supercontinent Rodinia formed at about 1100–1000 Ma and lasted approximately until 750 Ma ago (Pisarevsky *et al*., 2003). The similarity in palaeomagnetic data from the Buldelkhand craton of northern India with Eastern Dharwar craton of southern India indicates that these two cratons were in reasonable proximity at 1.0 Ga (Venkateshwarlu and Rao, 2013) and were part of Rodinia. Rodinia began to fragment at around 800-750 Ma with the separation of Australia, east Antarctica, south China, India and Siberia from Laurentia. Extensive dyke swarms emplaced at 780 Ma in western Laurentia may record the initial breakup of the Rodinia in this area (Harlan *et al*., 2003). Recent palaeomagnetic reconstruction suggests that the two continents, India and South China were united together along the western margin of the Rodinia supercontinent (Torsvik *et al*., 2001; Jiang *et al*.,

2003; Li *et al*., 2004; Duan *et al*., 2011). Hofmann *et al*. (2011) suggested that similarities between the detrital zircon ages of the Indian and the Chinese tillites and sandstones indicate that both areas shared a similar history in the Neoproterozoic. Considering the new geochronological data, the formation of the Badami–Bhima (and part of Kurnool) basins (800–900 Ma) is linked to the breakup of Rodinia supercontinent (Joy *et al*. (2018). The Neoproterozoic supercontinent fragmentation along with global scale flood basaltic eruptions resulted an initial increase of atmospheric greenhouse gases (Godderis *et al*., 2003; Hofmann *et al*., 2011). Later, increased weathering of exposed rocks and basaltic provinces subsequently consumed CO_2 through silicate weathering and reduced the atmospheric greenhouse gas levels (Godderis *et al*., 2003; Stern and Miller, 2018). Recent studies demonstrate that initial continental rifting can cause intensified CO_2 degassing (Ibs-von Seht et al., 2008; Brune *et al*., 2017) and injection of other greenhouse gases (Fischer, 2008; Jolie et al., 2016) to the atmosphere, which in turn can elevate the degree of chemical weathering under a hot, humid climate. Therefore, the interpretation of climate-induced transformation from ephemeral to perennial fluvial system appears to be consistent with the tectonic record.

Geochemical investigations demonstrate that the source rock were K-rich granitoids or K-rich quartzo-feldspathic sediments, like the Saundatti Quartzite with fewer contributions from basalts, greywackes, shaley BIFs and phyllitic metasediments of the Archaean Chitradurga Schist Belt and Hungund-Kushtagi Schist Belt as revealed from the major oxide normalization with respect to PCS (Fig. 13B) and UCC (Fig. 13C). Further, values from Zr/Ni vs. Zr/Cr (Fig. 14C) and Cr vs Ni (Fig. 14D) suggest direct contribution from the Saundatti Quartzite. Minor contribution from mafic and iron rich sources of greenstone belts are recorded within products of debris flows along the southern margin. It is also supported by the occasional presence of chert, hematite and BHJ fragments within the conglomeratic

framework constituents (Fig. 6B). Thus, source mixing is quite evident, although Saundatti Quartzite appears to be the major provenance contributor.

The Kerur Formation, as a whole, is a fining-upward sequence containing coarser clastic deposit at the base and shale at top; the latter, with carbonates, constitute the overlying Katageri Formation. The studied basal segment of the Kerur Formation was deposited over an unconformity and is overlain by a marine deposits with a transgressive lag at the base, which can be interpreted as lowstand systems tract (LST) (Catuneanu, 2006; Figs. 1, 2). The progradation in the LST is most pronounced in the proximal section at the Gokak area (Fig. 9). The overall fining-upward fluvial succession of the Kerur Formation suggests fluvial channel aggradation, as a result of a slow rise in base profile (Sarkar *et al*., 2012). The marine body eventually transgressed the study area and drowned the fluvial deposits.

12. **CONCLUSIONS**

The basal interval of the Neoproterozoic Kerur Formation of the Badami Group is characterized by scree, alluvial fan and fluvial deposits in the western part of the basin. The fluvial systems associated with this fan evolved from ephemeral to semi-perennial to perennial down the slopes. The spatial flow duration within the fluvial systems is principally controlled by the water table fluctuation, which is more pronounced in an overall semi-arid climatic condition. However, climatic alteration resulted in a permanent rise of the water table thereby facilitating development of a semiperennial to perennial fluvial system higher in the succession all through the study area. Despite variations in flow duration, the channels are dominated by a braided pattern that is consistent with the vegetation-free Precambrian alluvial systems. The mode of sediment transport and deposition, facies and architectural element pattern and stratigraphic architecture is principally controlled by basin-margin

tectonics in both depositional dip- and strike- parallel directions. The northerly and southerly palaeoflow directions within the screecone and alluvial fan settings indicates that they have originated on both sides of the east-west trending basin margin fault system. However, the westerly palaeoflow direction within the associated fluvial systems suggests a different palaeoslope for the latter. These corroborate the intracratonic rift model for the Badami basin. Quantitative petrographic studies further demonstrate uplifted continental source for the sediments of the Badami basin. Major and trace element geochemistry and molar A-CN-K plots, CIA and palaeoweathering trends of sandy sediments clearly point towards source mixing. However, Sandhauti Quartzite appears to be the primary contributor. The studied interval of the Kerur Formation represents an LST product showing a progradational character in the proximal fan part. The fluvial deposits formed during a slow rise in base profile initially, that became more pronounced later. The Badami rifting is possibly associated with Rodinia supercontinent breakup.

Acknowledgements

PS and SM acknowledge the UGC start-up grant and DAE-BRNS, Govt. of India for financing related research project. All the authors acknowledge their respective department for infrastructural facilities. The authors are thankful to the editor Prof. Brian Jones and the anonymous reviewer for their valuable comments and suggestions.

REFERENCES

Alexander, J., Fielding, C.R., 2006. Coarse-grained floodplain deposits in the seasonal tropics: towards a better facies model. Journal of Sedimentary Research 76 (3), 539–556.

Allen, J.R.L., 1968. Current Ripples. North-Holland Publishing Co., Amsterdam, 433 p.

Amir, M., Paul, D., Singh, A., Gupta, S., Chabaux, F., Granet, M. and Balakrishnan, S., 2018. Link between climate and catchment erosion in the Himalaya during the late Quaternary. Chemical Geology 501, 68–76.

Best, J.L., Ashworth, P.J., Bristow, C.S., Roden, J., 2003. Three-dimensional sedimentary architecture of a large, mid-channel sand braid bar, Jamuna River, Bangladesh. Journalof Sedimentary Research 73 (4), 516–530.

Blair, T.C., McPherson, J.G., 1994. Alluvial fans and their natural distinction from rivers based on morphology, hydraulic processes, sedimentary processes, and facies assemblages. Journal of Sedimentary Research 64 (3a), 450–489.

Blatt, H., Middleton, G., Murray, R., 1980. Origin of Sedimentary Rocks, 2nd Edition. Prentice-Hall Inc., Englewood Cliffs, New Jersey, 782 p.

Blum, M., Tornqvist, T., 2000. Fluvial responses to climate and sea-level change: a review and forward. Sedimentology 47, 2–48.

Bose, P.K., Sarkar, S., Mukhopadhyay, S., Saha, B., Eriksson, P., 2008. Precambrian basin-margin fan deposits: Mesoproterozoic Bagalkot Group, India. Precambrian Research 162 (1-2), 264–283.

Bridge, J.S., 1993. The interaction between channel geometry, water flow, sediment transport and deposition in braided rivers. In: Best, J.L., Bristow, C.S. (Eds.), Braided Rivers. Geol. Soc. Lond. Spec. Publ. 75, pp. 13–72.

Bridge, J.S., 2003. Rivers and Floodplains. Blackwell Scientific, Oxford, 504p.

Bridge, J.S., 2006. Fluvial facies models: recent developments. Special Publication-SEPM 84, 85–170.

Bromley, M.H., 1991. Architectural features of the Kayenta Formation (Lower Jurassic), Colorado Plateau, USA: relationship to salt tectonics in the Paradox Basin. Sedimentary Geology 73(1-2), 77–99.

Brune, S., Williams, S.E. and Mueller, R.D., 2017. Potential links between continental rifting, CO 2 degassing and climate change through time. Nature Geoscience 10(12), 941–946.

Buck, S.G., Minter, W.E.L., 1985. Placer formation by fluvial degradation of an alluvial fan sequence: the Proterozoic Carbon Leader placer, Witwatersrand Supergroup, South Africa. Journal of the Geological Society 142(5), pp.757–764.

Cant, D.J., 1978. Development of a facies model for sandy braided river sedimentation: Comparison of the South Saskatchewan River and the Battery Point Formation. Can. Soc. Petrol. Geol. Mem. 5, 627–639.

Catuneanu, O., 2006. Principles of Sequence Stratigraphy. Elsevier, Amsterdam, 375p.

Collinson, J.D., 1996. Alluvial sediments, In: Reading, H.G. (Ed.), Sedimentary Environments: Processes, Facies and Stratigraphy, 3rd Edition, Blackwell Science, Oxford, 37-82.

Collinson, J.D., & Thompson, D.B., 1989. Sedimentary Structure, 2nd edition. Unwin Hyman, London, 207 p.

Condie, K.C., 1993. Chemical composition and evolution of the upper continental crust: contrasting results from surface samples and shales. Chemical geology 104(1-4), pp.1–37.

Dam, G., Andreasen, F., 1990. High-energy ephemeral stream deltas; an example from the Upper Silurian Holmestrand Formation of the Oslo Region, Norway. Sedimentary Geology 66(3-4), 197–225.

Das, S., Goswami, B., Basak, A. and Bhattacharyya, C., 2020. A Grenvillian magmatic almandine garnet-bearing ferroan granite intrusion in the Chhotanagpur Gneissic complex, Eastern India: Petrology, petrochemistry, petrogenesis and geodynamic implications. Lithos 376, p. 105749.

Davis, A.M., Aitchison, J.C., Badengzhu, Luo, H., Zyabrev, S., 2002. Paleogeneisland arc collision-related conglomerates, Yarlung-Tsangpo suture zone, Tibet. Sediment. Geol. 150, 247–273.

Dey, S., Rai, A.K., Chaki, A., 2009. Palaeoweathering, composition and tectonics of provenance of the Proterozoic intracratonic Kaladgi–Badami basin, Karnataka, southern India: evidence from sandstone petrography and geochemistry. J. Asian Earth Sci. 34, 703–715.

Dey, S., 2015. Geological history of the Kaladgi–Badami and Bhima basins, south India: sedimentation in a Proterozoic intracratonic setup. Geological Society of London Memoirs 43(1), 283 – 296.

Dickinson, W.R. and Suczek, C.A., 1979. Plate tectonics and sandstone compositions. Aapg Bulletin 63(12), 2164–2182.

Dickinson, W.R., Beard, L.S., Brakenridge, G.R., Erjavec, J.L., Ferguson, R.C., Inman, K.F., Knepp, R.A., Lindberg, F.A. and Ryberg, P.T., 1983. Provenance of North American Phanerozoic sandstones in relation to tectonic setting. Geological Society of America Bulletin 94(2), 222–235.

Dickinson, W.R., 1985. Interpreting provenance relations from detrital modes of sandstones. In: Zuffa, G.G. (Ed.), Provenance of arenites. Springer, Dordrecht, pp. 333–361.

Duan, L., Meng, Q.R., Zhang, C.L. and Liu, X.M., 2011. Tracing the position of the South China block in Gondwana: U–Pb ages and Hf isotopes of Devonian detrital zircons. Gondwana Research 19(1), 141–149.

Duraiswami, R.A., Inamdar, M.M. and Shaikh, T.N., 2013. Emplacement of pillow lavas from the ~ 2.8 Ga Chitradurga Greenstone Belt, South India: A physical volcanological, morphometric and geochemical perspective. Journal of Volcanology and Geothermal Research 264, 134–149.

Eberth, D.A., & Miall, A. D. (1991). Stratigraphy, sedimentology and evolution of a vertebrate-bearing, braided to anastomosed fluvial system, Cutler Formation (Permian-Pennsylvanian), north-central New Mexico. Sedimentary Geology 72(3-4), 225–252.

Els, B.G., 1998. The question of alluvial fans in the auriferous Archean and Proterozoic successions of South Africa. S. Afr. J. Geol. 101, 17–25.

Eriksson, P.G., Bumby, A.J., Brümer, J.J., van der Neut, M., 2006. Precambrian fluvial deposits: enigmatic palaeohydrological data from the c. 2-1.9 Ga Waterberg Group, South Africa. Sediment. Geol. 190, 25–46.

Fedo, C.M., Wayne Nesbitt, H. and Young, G.M., 1995. Unraveling the effects of potassium metasomatism in sedimentary rocks and paleosols, with implications for paleoweathering conditions and provenance. Geology 23(10), 921–924.

Fielding, C.R., 1993. A review of recent research in fluvial sedimentology. Sedimentary Geology 85, 3–14.

Fielding, C.R., 2006. Upper flow regime sheets, lenses and scour fills: extending the range of architectural elements for fluvial sediment bodies. Sedimentary Geology 190(1-4), 227–240.

Fisher, R.V., 1971. Features of coarse-grained, high concentration fluids and their deposits. J. Sediment. Petrol. 41, 916–927.

Fischer, T.P., 2008. Fluxes of volatiles (H2O, CO2, N2, Cl, F) from arc volcanoes. Geochemical Journal 42(1), 21–38.

Frostick, L.E., Reid, I., 1977. The origin of horizontal laminae in ephemeral stream channel- fill. Sedimentology 24(1), 1–9.

Frostick, L.E., Reid, I., 1989. Climate versus tectonic controls of the fan sequences: lessons from the Dead Sea. Isr. J. Geol. Soc. 146, 527–538.

Gani, M.R., Alam, M.M., 2004. Fluvial facies architecture in small-scale river systems in the Upper DupiTila Formation, northeast Bengal Basin, Bangladesh. J. Asian Earth Sci. 24, 225–236.

Gao, C., Boreham, S., Preece, R.C., Gibbard, P.L., Briant, R.M., 2007. Fluvial response to rapid climate change during the Devensian (Weichselian) Late glacial in the River Great Ouse, southern England, UK. Sed. Geol. 202, 193–210.

Goddéris, Y., Donnadieu, Y., Nédélec, A., Dupré, B., Dessert, C., Grard, A., Ramstein, G. and François, L. M., 2003. The Sturtian 'snowball" glaciation: Fire and ice. Earth and Planetary Science Letters 211, 1–12.

Hallam, A., 1981. Facies interpretation and the stratigraphic record. W.H. Freeman and Company, San Francisco, 291 p.

Harlan, S.S., Heaman, L., LeCheminant, A.N. and Premo, W.R., 2003. Gunbarrel mafic magmatic event: A key 780 Ma time marker for Rodinia plate reconstructions. Geology 31(12), 1053–1056.

Harms, J.C., Fahnstock, R.K., 1965. Stratification, bedforms and flow phenomena (with an example from the Rio Grande). In: Middleton, G.V. (Ed.), Primary Sedimentary Structures and their Hydrodynamic Interpretation. Soc. Econ. Paleontol. Mineral., Spec. Publ. 12, 84–115.

Harms, J.C., Southard, J.B., Spearing, D.R., Walker, R.G., 1975. Depositional environments as interpreted from primary sedimentary structures and stratification sequences. Dallas: SEPM Short Course 2, 161 p.

Hassan, M.A., 2005. Characteristics of gravel bars in ephemeral streams. Journal of Sedimentary Research 75, 29–42.

Hegde, G.V., Pujar, G.S., Bhimesen, K., Gokhale, N.W., 1994. The Kaladge basin: A review. Geo Karnataka, NGD Centenary Volume, pp. 216–226.

Hjellbakk, A., 1997. Facies and fluvial architecture of a high-energy braided river: The Upper Proterozoic Seglodden Member, Varanger Peninsula, northern Norway. Sedimentary Geology 114, 131–161.

Hofmann, M., Linnemann, U., Rai, V., Becker, S., Gärtner, A. and Sagawe, A., 2011. The India and South China cratons at the margin of Rodinia—Synchronous Neoproterozoic magmatism revealed by LA-ICP-MS zircon analyses. Lithos 123(1-4), 176–187.

Holbrook, J., 2001. Origin, genetic interrelationships, and stratigraphy over the continuum of fluvial channel-form bounding surfaces: an illustration from middle Cretaceous strata, southeastern Colorado. Sediment. Geol. 144, 179–222.

Hooke, R.L., 1967. Processes on arid-region alluvial fans. The Journal of Geology 75(4), 438–460.

Ibs-von Seht, M., Plenefisch, T. and Klinge, K., 2008. Earthquake swarms in continental rifts—A comparison of selected cases in America, Africa and Europe. Tectonophysics 452(1-4), 66–77.

Jayaprakash, A.V., Sundaram, V., Hans, K., Mishra, R.N., 1987. Geology of the Kaladgi–Badami Basin, Karnataka. In: Radhakrishna, B.P. (Ed.), Purana Basins of Peninsular India (middle to late Proterozoic). Mem. Geol. Soc. Ind. 6, 201–225.

Jiang, G., Sohl, L.E. and Christie-Blick, N., 2003. Neoproterozoic stratigraphic comparison of the Lesser Himalaya (India) and Yangtze block (south China): Paleogeographic implications. Geology 31(10), 917–920.

Jolie, E., Klinkmueller, M., Moeck, I. and Bruhn, D., 2016. Linking gas fluxes at Earth's surface with fracture zones in an active geothermal field. Geology 44(3), 187–190.

Joy, S., Patranabis- Deb, S., Saha, D., Jelsma, H., Maas, R., Söderlund, U., Tappe, S., van Der Linde, G., Banerjee, A. and Krishnan, U., 2019. Depositional history and provenance of cratonic "Purana" basins in southern India: A multipronged geochronology approach to the Proterozoic Kaladgi and Bhima basins. Geological Journal 54(5), 2957–2979.

Kale, V.S., Phansalkar, V.G., 1991. Purana basins of peninsular India: a review. Basin Research 3(1), 1–36.

Kale, V.S., 1995. Association of the Purana basins and the Middle Proterozoic mobile belts in Peninsular India: implications on targeting uranium deposits. Exploration and Research for Atomic Minerals 8, 95–2110.

Kirk, M., 1983. Bar development in a fluvial sandstone (West-phalian 'A'), Scotland. Sedimentology 30, 727–742.

Lamminen, J., Köykkä, J., 2010. The provenance and evolution of the Rjukan Rift Basin, Telemark, south Norway: The shift from a rift basin to an epicontinental sea along a Mesoproterozoic supercontinent. Precambrian Research 181, 129–149.

Li, Z.X., Evans, D.A.D. and Zhang, S., 2004. A 90 spin on Rodinia: possible causal links between the Neoproterozoic supercontinent, superplume, true polar wander and low-latitude glaciation. Earth and Planetary Science Letters 220(3-4), 409–421.

Long, D.G.F., 2004. Precambrian Rivers. In: Eriksson, P.G., Altermann, W., Nelson, D.R., Mueller, W.U., Catuneanu, O. (Eds.), The Precambrian Earth: Tempos and Events. Elsevier, Amsterdam, pp. 660–663.

Long, D.G.F., 2006. Architecture of pre-vegetation sandy-braided perennial and Ephemeral River deposits in the Paleoproterozoic Athabasca Group, northern Saskatchewan, Canada as indicators of Precambrian fluvial style. Sed. Geol. 190 (1–4), 71–95.

Long, D.G.F., 2011. Architecture and depositional style of fluvial systems before land plants: a comparison of Precambrian, early Paleozoic, and modern river deposits. In: North, C. (Ed.), From River to Rock Record: The Preservation of Fluvial Sediments and their Subsequent Interpretation. SEPM Spec. Publ. 97, pp. 37–61.

Lowe, D.R., 1976. Grain flow and grain flow deposits. J. Sediment. Petrol. 46, 188–190.

Lowe, D., 1979. Sediment gravity flows: their classification and some problems of application to natural flows and deposits. Geology of Continental Slopes 27, 75–82.

Mahanta, B.N., Pal, T., Bhardwaj, A., 2019. Basin margin fan-delta deposits of the Cretaceous sediments of Meghalaya, India- a hint for Gondwana breakup. Indian Journal of Geosciences 73(2), 89–94.

Mazumder, R., Sarkar, S., 2004. Sedimentation history of the Palaeoproterozoic Dhanjori Formation, Singhbhum, eastern India. Precambrian Research 130(1-4), 267–287.

Miall, A.D., 1980. Cyclicity and the facies model concept in fluvial deposits. Bulletin of Canadian Petroleum Geology 28(1), 59–79.

Miall, A.D., 1981. Analysis of fluvial depositional systems. In: Education Course Note Series- 20. American Association of Petroleum Geologists, 75 p.

Miall, A.D., 1985. Architectural-element analysis: a new method of facies analysis applied to fluvial deposits. Earth Science Reviews 22, 261–308.

Miall, A.D., 1988. Architectural elements and bounding surfaces in fluvial deposits: anatomy of the Kayenta Formation (Lower Jurassic), southwest Colorado. Sedimentary Geology 55(3-4), 233–262.

Miall, A.D., 1994. Reconstructing fluvial macroform architecture from two-dimensional outcrops; examples from the Castlegate Sandstone, Book Cliffs, Utah. Journal of Sedimentary Research 64 (2b), 146–158.

Miall, A.D., 1996. The Geology of Fluvial Deposits: Sedimentary Facies, Basin Analysis and Petroleum Geology. Springer, New York, 582p.

Miall, A.D., Jones, B., 2003. Fluvial architecture of the Hawkesbury Sandstone (Triassic), near Sydney, Australia. J. Sediment. Res. 73, 531–545.

Miall, A.D., 2006. How do we identify big rivers? And how big is big? Sedimentary Geology 186, 39–50.

Miall, A.D., 2014. Fluvial depositional systems, Vol. 14. Springer International Publishing, Berlin, 316 p.

Middleton, 1970. Experimental studies related to problems of flysch sedimentation, In: Lajoie, J. (Ed.), Flysch Sedimentology in North America, Geol. Soc. Canada Spec. Paper, 7, pp. 253–272.

Middleton, G.V., Hampton, M.A., 1973. Sediment gravity flows: mechanics of flow and deposition, In: Middleton, G.V., Bouma, A.H. (Eds.), Turbidites and Deep-Water Sedimentation. Soc. Econ. Paleontologists Mineralogists, Pacific Section, Short Course Lecture Notes, pp. 1–38.

Middleton, G.V., Hampton, M.A., 1976. Subaqueous sediment transport and deposition by sediment gravity flows. In: Stanley, D.J., Swift, D.J.P. (Eds.), Marine sediments, transport and environmental management. John Wiley, New York, pp. 197–219.

Milana, J.P., 2010. The sieve lobe paradigm: Observations of active deposition. Geology 38 (3), 207–210.

Mukhopadhyay, S., Choudhuri, A., Samanta, P., Sarkar, S., Bose, P. K., 2014. Were the hydraulic parameters of Precambrian rivers different? Journal of Asian Earth Sciences 91, 289–297.

Mukhopadhyay, S., Samanta, P., Bhattacharya, S., Sarkar, S., 2019. Stratigraphic evolution and architecture of the terrestrial succession at the base of the Neoproterozoic Badami Group, Karnataka, India. In: Mondal, M.E.A. (Ed), Geological evolution of the Precambrian Indian shield. Springer, pp. 121–157.

Naqvi, S.M., Sawkar, R.H., Rao, D.S., Govil, P.K. and Rao, T.G., 1988. Geology, geochemistry and tectonic setting of Archaean greywackes from Karnataka Nucleus, India. Precambrian Research 39(3), 193–216.

Naqvi, S.M., Khan, R.M.K., Manikyamba, C., Mohan, M.R. and Khanna, T.C., 2006. Geochemistry of the NeoArchaean high-Mg basalts, boninites and adakites from the Kushtagi–Hungund greenstone belt of the Eastern Dharwar Craton (EDC); implications for the tectonic setting. Journal of Asian Earth Sciences 27(1), 25–44.

Nesbitt, H.W. and Young, G.M., 1984. Prediction of some weathering trends of plutonic and volcanic rocks based on thermodynamic and kinetic considerations. Geochimica et Cosmochimica Acta 48(7), 1523–1534.

Nesbitt, H.W. and Young, G.M., 1989. Formation and diagenesis of weathering profiles. The Journal of Geology 97(2), 129–147.

Nesbitt, H.W., Young, G.M., McLennan, S.M. and Keays, R.R., 1996. Effects of chemical weathering and sorting on the petrogenesis of siliciclastic sediments, with implications for provenance studies. The Journal of Geology 104(5), 525–542.

Nemec, W., Steel, R.J., 1984. Alluvial and coastal conglomerates: their significant features and some comments on gravelly mass-flow deposits. In: Koster, E.H., Steel, R.J. (Eds.), Sedimentology of Gravels and Conglomerates. Can. Soc. Pet. Geol. Mem. 10, pp. 1–31.

Nichols, G., Thompson, B., 2005. Bedrock lithology control on contemporaneous alluvial fan facies, Oligo-Miocene, southern Pyrenees, Spain. Sedimentology 52, 571–585.

Nilsen, T.H. (Ed.), 1985. Modern and ancient alluvial fan deposits. Benchmark Papers in Geology 87. Van Nostrand Reinhold, New York.

Olsen, J.C., 1987. Tectonic evolution of the North Sea region. In: Conference on petroleum geology of North West Europe 3, pp. 389–401.

Olsen, H., 1989. Sandstone-body structures and ephemeral stream processes in the Dinosaur Canyon Member, Moenave Formation (Lower Jurassic), Utah, U.S.A. Sediment. Geol. 61, 207–221.

Patil Pillai, S., Pande, K. and Kale, V.S., 2018. Implications of new $^{40}Ar/^{39}Ar$ age of Mallapur Intrusives on the chronology and evolution of the Kaladgi Basin, Dharwar Craton, India. Journal of Earth System Science 127(3), 1–18.

Pettijohn, F.J., 1975. Sedimentary rocks, 3rd edition, Harper and Row, New York. 628p.

Pfluger, F., Seilacher, A., 1991. Flash flood conglomerates. In: Einsele, G., Ricken, W., Seilacher, A. (Eds.), Cycles and Events in Stratigraphy, Springer, Berlin, pp. 383–391.

Picard, M.D., High, L.R., 1973. Sedimentary structures of ephemeral streams. Elsevier Science, 222 p.

Pisarevsky, S.A., Wingate, T.D., Powell, C.McA., Johnson, S., Evans, D.A.D., 2003. Models of Rodinia assembly and fragmentation. Proterozoic East Gondwana: Supercontinent Assembly and Breakup: In: Yoshida, M., Windley, B.F., Dasgupta, S. (Eds.), Geological Society London, Special Publication 206, pp. 35–55.

Posamentier, H.W., Walker, R.G., 2006. Deep-water turbidites and submarine fans. In: Posamentier, H.W., Walker, R.G. (Eds.), Facies models revisited. Society for Economic geology, Palaeontology and Mineralogy (Special Publication 84), pp. 399–520.

Raha, P.K., Sastry, M.V.A., 1982. Stromatolites and Precambrian Stratigraphy in India. Precambrian Res. 18, 293–318.

Rao, T.G. and Naqvi, S.M., 1995. Geochemistry, depositional environment and tectonic setting of the BIF's of the late Archaean Chitradurga schist belt, India. Chemical Geology 121(1-4), 217–243.

Reading, H.G., 1986. Sedimentary environments and facies, 2nd Ed., Blackwell, Oxford, 524 p.

Rudnick, R.L. and Gao, S., 2003. Composition of the Continental Crust. Treatise on Geochemistry 3, 659 p.

Rust, B.R., Koster, E.H., 1984. Coarse alluvial deposits. In: Walker, R.G. (Ed.), Facies Models, second ed., Geological Association of Canada, Toronto, pp. 53–69.

Rygel, M.C., Gibling, M.R., 2006. Natural geomorphic variability recorded in a high-accommodation setting: fluvial architecture of the Pennsylvanian Joggins Formation of Atlantic Canada. Journal of Sedimentary Research 76 (11), 1230–1251.

Samanta, P., Mukhopadhyay, S., Eriksson, P.G., 2016. Forced regressive wedge in the Mesoproterozoic Koldaha Shale, Vindhyan basin, Son valley, central India. Marine and Petroleum Geology 71, 329–343.

Sarkar, S., Samanta, P., Mukhopadhyay, S., Bose, P.K., 2012. Stratigraphic architecture of the Sonia Fluvial interval, India in its Precambrian context. Precambrian Res. 214–215, 210–226.

Schumm, S.A., 1968. Speculations concerning palaeohydrologic controls of terrestrial sedimentation. Geological Society of America Bulletin 79, 1573-1588.

Selley, R.C., 1965. Diagnostic characters of fluviatile sediments of the Torridonian formation (Precambrian) of northwest Scotland. J. Sediment. Res. 35, 366–380.

Simons, D.B., Richardson, E.V., Nordin JR., C.F., 1965. Sedimentary structures generated by flow in alluvial channels. In: Middleton, G.V. (Ed.), Primary Sedimentary Structures and Their Hydrodynamic Interpretation. Soc. Econ. Paleontologists Mineralogists Spec. Publ. 12, 34–52.

Smith, G.A., 1986. Coarse-grained nonmarine volcaniclastic sediment: terminology and depositional process. Geol. Soc. Am. Bull., 97, 1–10.

Smith, N.D., Rogers, J., 1999. Fluvial sedimentology, ed. VI, Blackwell Sciences, Oxford, 478 p.

Sridhar, M., Chaturvedi, A.K. Rai, A.K., 2014. Locating new uranium occurrence by integrated weighted analysis in Kaladgi basin, Karnataka. Journal of the Geological Society of India 84 (5), 509–512.

Stern, R.J. and Miller, N.R., 2018. Did the transition to plate tectonics cause Neoproterozoic Snowball Earth? Terra Nova 30(2), 87–94.

Taylor, S.R., and McLennan, S.M., 1985. The Continental Crust: Its Composition and Evolution. Oxford, Blackwell.

Torsvik, T.H., Carter, L.M., Ashwal, L.D., Bhushan, S.K., Pandit, M.K. and Jamtveit, B., 2001. Rodinia refined or obscured: palaeomagnetism of the Malani igneous suite (NW India). Precambrian Research 108(3-4), 319–333.

Tunbridge, I.P., 1981. Sandy high-energy flood sedimentation—some criteria for recognition, with an example from the Devonian of SW England. Sedimentary Geology 28 (2), 79–95.

Tunbridge, I.P., 1984. Facies model for a sandy ephemeral stream and clay playa complex; the Middle Devonian Trentishoe Formation of North Devon, UK. Sedimentology 31 (5), 697–715.

Venkateshwarlu, M., Rao N.V.C., 2013. New palaeomagnetic and rock magnetic results on Mesoproterozoic kimberlites from the Eastern Dharwar craton, southern India: Towards constraining India's position in Rodinia. Precambrian Research 224, 588 - 596.

Walker, R.G., 1984. Shelf and shallow marine sands. In: Walker, R.G. (ed.), Facies Models. Geoscience Canada Reprint Series 1, 141–170.

Wasson, R.J., 1974. Intersection point deposition on alluvial fans: an Australian example. Geografiska Annaler 56A (1-2), 83 – 92.

Waters, J.V., Jones, S.J. and Armstrong, H.A., 2010. Climatic controls on late Pleistocene alluvial fans, Cyprus. Geomorphology 115 (3-4), 228–251.

Wei, G.J., Liu, Y., Li, X.H., 2004. Major and trace element variations of the sediments at ODP Site 1144, South China Sea, during the last 230 ka and their paleoclimate implications. Palaeogeography, Palaeoclimatology, Palaeoecology 212, 331–342.

Yan, Y., Xia, B., Lin, G., Cui, X., Hu, X., , Yan, P., Zhang, F., 2007. Geochemistry of the sedimentary rocks from the Nanxiong Basin, South China and implications for provenance, paleoenvironment and paleoclimate at the K/T boundary. Sedimentary Geology 197, 127-140.

Yu, X., Ma, X., Quing, H., 2002. Sedimentology and reservoir characteristics of a Middle Jurassic fluvial system, Datong Basin, northern China. Bulletin of Canadian Petroleum Geology 50 (1), 105–117.

Figure Captions

Fig. 1. Location and Geological background of the study area: Geological map displaying the spatial distribution of different stratigraphic units of the Kaladgi basin including the Archaean basement rocks with some important faults and cross faults. Study area has been marked by a rectangle. Note relevant part of Indian map within inset (modified after Jayaprakash *et al*.,

1987) (A). Geophysical reconstruction of the E - W trending Kaladgi basin bounded by basin margin faults on the north and south. Note the occurrence of other E – W to NE – SW trending faults and NNE – SSW trending cross faults (modified after Sridhar *et al*., 2014). The spatial distribution of different stratigraphic units shown as outcrop boundaries (modified after Jayaprakash *et al*., 1987). Also note the study locations represented by numbers (S1 to S7) used in figs. 8, 9, 11 and 12 (B). The rectangular area on the extreme lower right corner in fig. 1B is highlighted displaying detailed locations used in fig. 8 (C).

Fig. 2. General stratigraphy of the Kaladgi Supergroup (after Jayaprakash *et al*., 1987), divided into the Bagalkot and the Badami Group in ascending order. Note bipartite division of the Badami Group and further subdivisions of the Kerur Formation into four lithological units. Relevant stratigraphic interval and its sequence stratigraphic status shown on the right.

Fig. 3. Facies A: Highly angular clast supported breccia with jagged lower contact due to penetration of clasts. Note the reclined clasts marked by double headed arrows. Also note occurrence of thin granular sandstone of fan-apron origin (subfacies G_2) marked by dotted lines on the middle (A). Matching boundaries of broken clasts marked by rectangles (B). Deep penetration of clasts into the lower sandy beds. Note crude cross strata in granular sandstone of subfacies G_2 just below the dotted line (C). Facies B: Matrix supported conglomerate with haphazard orientations of clasts. Note protrusion of clast marked by arrows. Also note sharp base, marked by dotted line, and slight upward convexity of the SGE (D). Facies C: Clast supported conglomerate with occasional reverse grading marked by arrows. Note bed boundaries highlighted by dotted lines (E). Facies D: Clast supported conglomerate giving rise to sandstone upward because of sand infiltration. Note upward convexity of the unit marked by dotted lines. Also note crude cross strata towards top (F).

Fig. 4. Facies E: Clast supported conglomerate with preferred leftward intermediate axis imbrication of clasts (A). Facies F: Clast supported lenticular massive conglomerate with erosional base and flat top representing channel thalweg marked by dotted lines. Note overlying trough cross stratified channel sandstone with sharp contact (B). Subfacies G_1: Very coarse grained lenticular massive to crudely cross stratified (highlighted by solid lines on right top) sandstone bodies, marked by dotted lines, with sharp base and convex-up top. Note occurrence of oversized clasts floating on the SGE (C). Subfacies G_2: Very coarse grained lenticular massive sandstone bodies associated with scree breccia facies (D). Subfacies H_1: Pebbly trough cross stratified sandstone, representative of SCE. Note lack of master erosion surface within the channel bodies (E). Subfacies H_2: Very coarse to medium grained trough cross stratified sandstone, representative of SCE. Note pebbles are concentrated on the trough bases marked by arrows (F).

Fig. 5. Subfacies H_3: Pebble free, medium to fine grained lenticular trough cross stratified sandstone. Note erosional base of the channel body marked by dotted line of the SCE (A). Facies I: Compound cross stratified sandstone facies (DAE in oblique section) in between two trough cross stratified sandstones. Note upward convexity and flat base of the unit. Also note palaeocurrent roses for large (solid) and small (open) scale cross strata oriented in the same direction (B). Subfacies J_1: Massive to planar laminated sandstone, representative of LSE, overlying compound cross stratified sandstone with sharp contact marked by dotted line. Note some planar laminae highlighted by solid lines (C). Subfacies $J_{2:}$ Planar laminated sandstone (representative of LSE), marked by dotted lines, overlying trough cross stratified channel sandstone with sharp contact (D). Facies K: Ripple laminated sandstone (representative of LSE), marked by arrow, on top of trough cross stratified channel sandstone

(E). Subfacies L_1: Tabular cross stratified sandstone corresponds to LAE underlying compound cross stratified sandstone. Note the palaeocurrent roses for tabular cross strata (open) are oriented at high angle to the associated trough and compound cross strata (solid) (F).

Fig. 6. Subfacies L_2: Large tabular cross stratified sandstone, representative of TBE, overlying master erosion surface. Note the palaeocurrent roses of tabular cross strata (open) oriented at the same direction to the associated trough and compound cross strata (solid) (A). Clast composition of breccia and conglomerate (rudaceous facies association 1 and 2) at three different study locations, namely, Murgod, Deshnur and Gokak (see fig. 1). Note the clast composition of breccia and conglomerate in facies association 2 at Deshnoor and Gokak shows wider spectrum than facies association 1 at Murgod (B). Photomicrograph of very coarse to coarse grained feldspar rich matrix of clast-supported scree conglomerate (facies A) of facies association 1. Note ill-sorted subrounded grains with high textural immaturity. Ch: chert clast, Mc: microcline, K-pr: clast of k-feldspar showing perthitic intergrowth (C). Photomicrograph of matrix of matrix-supported debris flow conglomerate (facies B) of facies association 1 made up of quartz, feldspar and clay minerals. Note the presence of illitic (IL) matrix and calcitic (Ca) cement. Pl: plagioclase, Or: orthoclase, Mc: microcline, K-pr: clast of K-feldspar showing perthitic intergrowth (D). Photomicrograph of arkosic arenite from facies association 2 (subfacies H_1) with angular to subangular coarse, sand-sized grains having moderate to poor sorting (E). Photomicrograph of poorly sorted arkosic arenite from facies association 3 (subfacies J_2) with coarse to medium sand sized mono and polycrystalline quartz, unaltered orthoclase, microcline and plagioclase feldspar with lithic fragments of chert and quartzite (Qtz) (F).

Fig. 7. Photomicrograph of poorly sorted subarkosic arenites from facies association 4 (subfacies H_2) with subrounded to subangular, coarse to medium sand sized feldspar and quartz grains (A). Soft sediment deformation structures within facies association 4: overturned cross strata. Note the structure is highlighted above by sketch (B), water escape structures marked by arrows (C). Storeys of sandstone in facies associations 4 and 5. Note the sketch traces of bounding surfaces of different orders. Also note that the channel belts in facies association 5 are thinner and sheet like in comparison to facies association 4 (D). Photomicrograph of subarkosic arenite from facies association 5 with altered feldspar grains (illitic alteration) under plane polarized (E) and cross polarized light (F). Photomicrograph of texturally matured, moderate to well sorted quartz arenite having medium sand-sized framework grains from channel sandstones (subfacies H_3) of facies association 5 (G). Soft sediment deformation structure within stratigraphic package 1 (facies association 3): convolute laminations (H).

Fig. 8. Facies distribution in three sections moving along the dip direction from left to right at locality Murgod (see fig. 1C for location) clearly showing wedge like scree deposit. Clast composition of different facies at the right bottom. Note palaeocurrent orientation of different sandy facies and facies associations. Symbols used for the facies comprising the stratigraphic segments in all three locations are presented at the left bottom.

Fig. 9. Facies distribution at locality Gokak (see fig. 1 for location) highlighting the vertical variation in facies of a prograding alluvial fan and associated fluvial deposits. Clast composition of conglomerates and breccias of different facies on the right. Note palaeocurrent orientation of different sandy facies association. Also note a few laterally extensive soft sediment deformation structures within the basal part of the stratigraphic

interval. Symbols used for the facies comprising the stratigraphic segment are presented at the bottom.

Fig. 10. The sharp contact between facies association 2 and 5 at locality Gokak. The lower trace highlighting the distribution of facies within facies association 2 in time and space.

Fig. 11. Facies distribution at locality Deshnur (see fig. 1 for location). Clast composition of different conglomeratic facies and palaeocurrent orientation of different sandy facies associations at right. Note laterally extensive soft sediment deformation structures at the basal part of facies association 5. Symbols used for the facies comprising the stratigraphic segment are presented at the bottom.

Fig.12. Facies distribution at localities Islampur and Gujanal (see fig. 1 for location). Note palaeocurrent orientation of facies association 4 and 5 are consistent. Also note laterally extensive soft sediment deformation structures at the basal part of facies association 5 at both localities. Symbols used for the facies comprising the stratigraphic segment are presented at the right bottom (A). Granitic basement below facies association 4 (B).

Fig. 13. Q_t-F-L triangular plot of 25 selected sandy specimens, after Dickinson (1985), to correlate the provenance characteristics and tectonic setup based on modal proportions of total quartz (Q_t), feldspar (F) and lithic fragments (L) in the framework. Note most of the data plotted within the "basement uplift" and "transitional continent" field (A). Normalization of the geochemical major oxide data of the representative 15 samples with respect to the average Proterozoic Cratonic Sandstone (PCS; Condie, 1993) (B) and average Upper Continental Crust (UCC; Taylor and McLennan, 1985; Rudnick and Gao, 2003) (C). Note that

exceptional trend of sample number 11of Table 1, BD-MU-5, is demarcated by red dots and red line and the average trend of the rest of the samples is demarcated by blue dots and blue dashed line (B, C). (K_2O + Na_2O) vs. K_2O/Na_2O ratio diagram comparing the data of representative 15 samples to the data from surrounding immediate basement rocks; Saundatti Quartzite (Dey *et al*., 2009), Peninsular Gneisses (PGC) (Dey *et al*., 2009), greywacke and phyllites from Chitradurga and Gadag Schist Belts (Naqvi *et al*., 1988), cherts, shales and BIFs from Chitradurga Schist Belt (CSB) (Rao and Naqvi, 1995), Chitradurga pillow basalts (Duraiswami *et al*., 2013), Closepet Granite (CG, Dey *et al*., 2009) and basalts of Hungund-Kushtagi schist belt (Naqvi *et al*., 2006; Dey *et al*., 2009) (D).

Fig. 14. SiO_2/Al_2O_3 ratio vs. (FeO_T + MgO)/(K_2O + Na_2O) ratio diagram comparing the data of representative 15 samples to the data from surrounding immediate basement rocks (A). Comparison of trace element data from of the representative 15 samples to the data from surrounding immediate basement rocks in Zr/Ni vs. Zr/Cr diagram (B) and Cr vs Ni diagram (C). A-CN-K molar triangular plot after Nesbitt and Young (1984, 1989) and Nesbitt *et al*. (1996) showing weathering trends of different provenances and their correlation with the representative 15 samples; black solid circle: facies association 1 and 2, black hollow triangle: facies association 3, grey solid triangle: facies association 4 and 5 (D).

Fig. 15. Cartoon displaying the inferred palaeoenvironmental distribution of the facies constituting the studied stratigraphic interval. The spatial distribution of scree-alluvial fan and fluvial package 1, 2 and 3 (SP 1, 2 and 3) shown in reference to water table and inferred slope control on distance from the basin margin. The occurrence of sieve represents possible highest level of water table (intersection point) and SP 2, 3 occur below water table saturation. Note that scree-alluvial fan and associated ephemeral fluvial systems (SP 1)

generated from either side of the basin margin fault system following local palaeoslopes, however, semi-perennial and perennial fluvial systems (SP 2 and 3) follow regional westerly palaeoslope.

Research highlights

1) Facies and architectural element analysis unravel paleogeography.
2) Control of flow durability within channels in time and spaced has been inferred.
3) Geochemistry, molar A-CN-K and palaeoweathering trends traced provenances.
4) Quantitative petrography, depositional model support synchronous Rodinia rifting.
5) Sequence stratigraphic status and stratigraphic architectural control delineated.

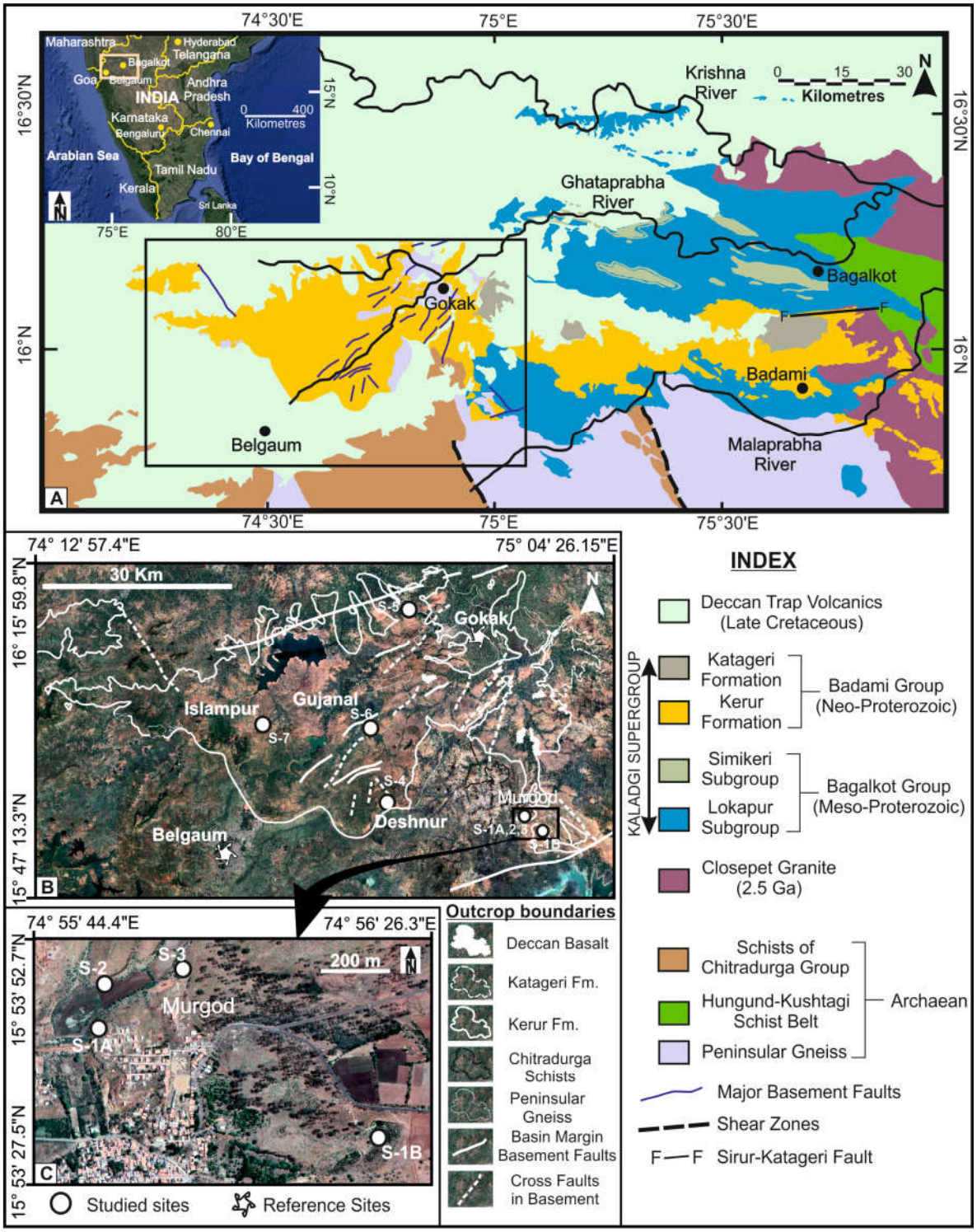
74°30'E
75°E
75°30'E
16°30'N
16°N
Maharashtra
Hyderabad
Telangana
Bagalkot
Goa
Belgaum
Andhra Pradesh
INDIA
Karnataka
Bengaluru
Chennai
Arabian Sea
Bay of Bengal
Tamil Nadu
Kerala
Sri Lanka
0 400 Kilometres
15°N
10°N
75°E
80°E
Krishna River
0 15 30 Kilometres
N
Ghataprabha River
Bagalkot
Gokak
F F
Badami
Belgaum
Malaprabha River
A
74° 12' 57.4"E
75° 04' 26.15"E
16° 15' 59.8"N
15° 47' 13.3"N
30 Km
S-5
Gokak
Islampur
Gujanal
S-6
S-7
S-4
Deshnur
Murgod
S-1A,2,3
S-1B
Belgaum
B
74° 55' 44.4"E
74° 56' 26.3"E
15° 53' 52.7"N
15° 53' 27.5"N
200 m
S-2
S-3
Murgod
S-1A
S-1B
C
Studied sites
Reference Sites
Outcrop boundaries
Deccan Basalt
Katageri Fm.
Kerur Fm.
Chitradurga Schists
Peninsular Gneiss
Basin Margin Basement Faults
Cross Faults in Basement
INDEX
Deccan Trap Volcanics (Late Cretaceous)
KALADGI SUPERGROUP
Katageri Formation
Kerur Formation
Badami Group (Neo-Proterozoic)
Simikeri Subgroup
Lokapur Subgroup
Bagalkot Group (Meso-Proterozoic)
Closepet Granite (2.5 Ga)
Schists of Chitradurga Group
Hungund-Kushtagi Schist Belt
Peninsular Gneiss
Archaean
Major Basement Faults
Shear Zones
F—F Sirur-Katageri Fault

Figure 1

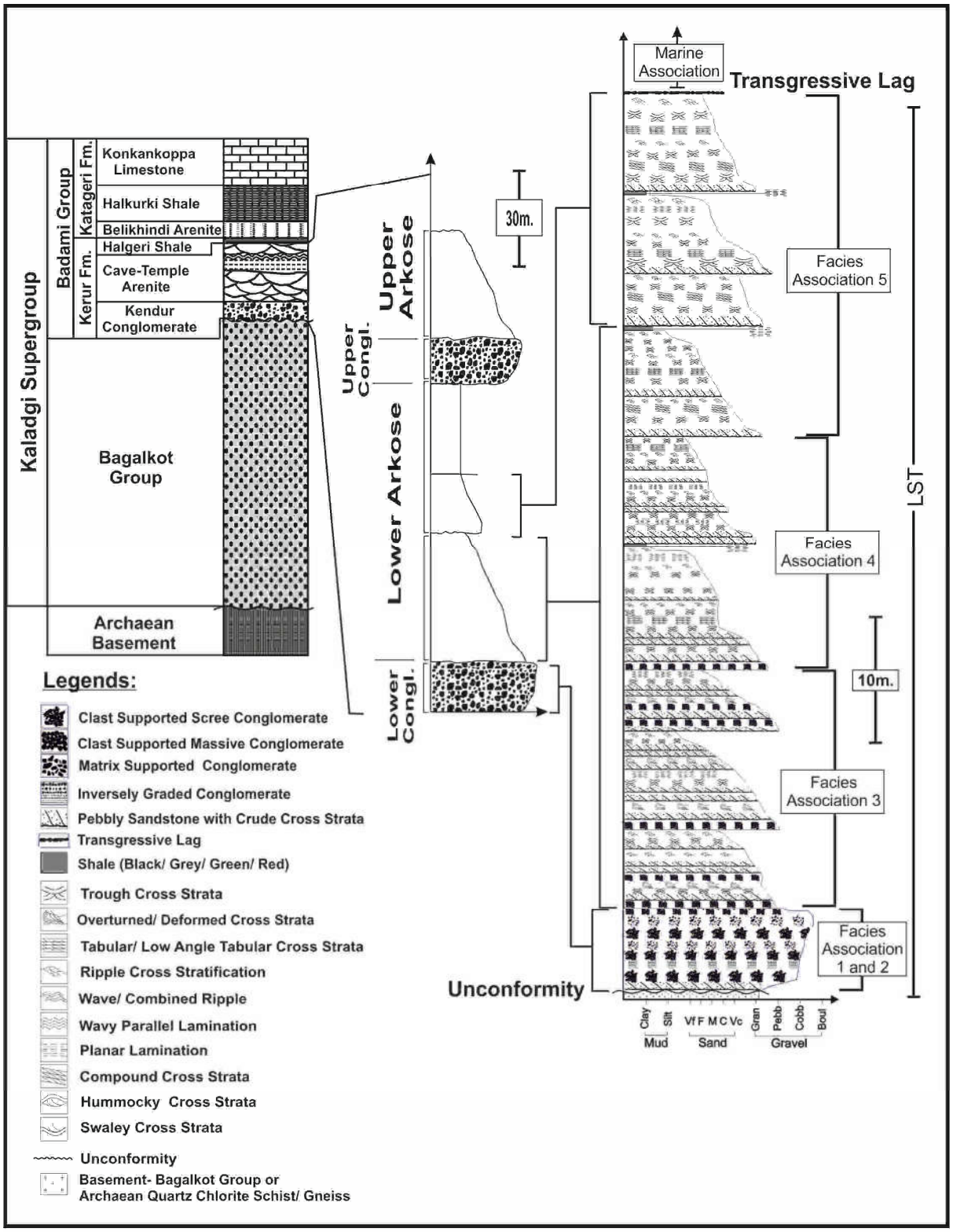
Kaladgi Supergroup
Badami Group
Katageri Fm.
Konkankoppa Limestone
Halkurki Shale
Belikhindi Arenite
Kerur Fm.
Halgeri Shale
Cave-Temple Arenite
Kendur Conglomerate
Bagalkot Group
Archaean Basement
Upper Arkose
Upper Congl.
Lower Arkose
Lower Congl.
30m.
10m.
Marine Association
Transgressive Lag
Facies Association 5
Facies Association 4
Facies Association 3
Facies Association 1 and 2
LST
Unconformity
Clay Slit VfF MC Vc Gran Pebb Cobb Boul
Mud Sand Gravel
Legends:
Clast Supported Scree Conglomerate
Clast Supported Massive Conglomerate
Matrix Supported Conglomerate
Inversely Graded Conglomerate
Pebbly Sandstone with Crude Cross Strata
Transgressive Lag
Shale (Black/ Grey/ Green/ Red)
Trough Cross Strata
Overturned/ Deformed Cross Strata
Tabular/ Low Angle Tabular Cross Strata
Ripple Cross Stratification
Wave/ Combined Ripple
Wavy Parallel Lamination
Planar Lamination
Compound Cross Strata
Hummocky Cross Strata
Swaley Cross Strata
Unconformity
Basement- Bagalkot Group or Archaean Quartz Chlorite Schist/ Gneiss

Figure 2

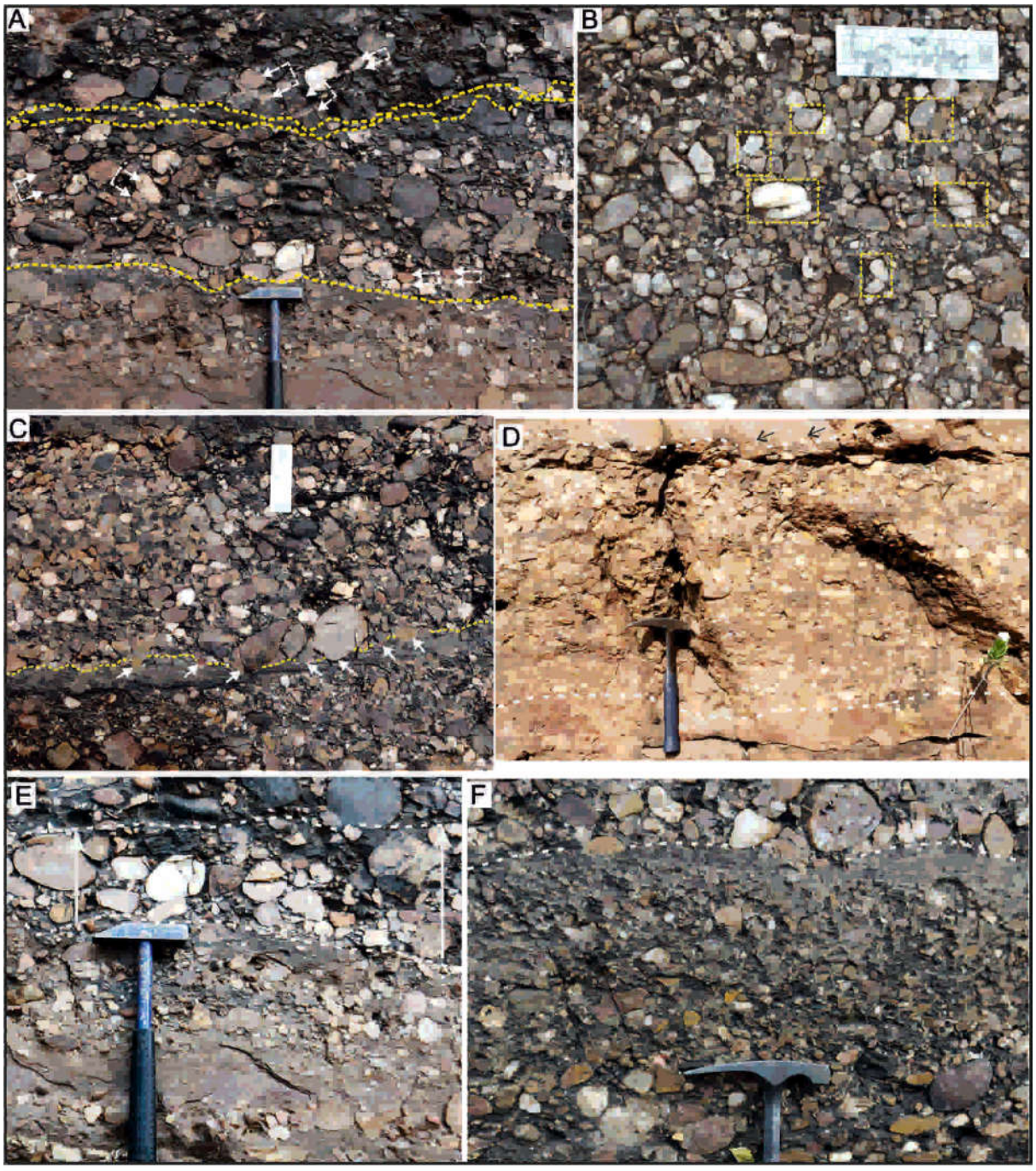

Figure 3

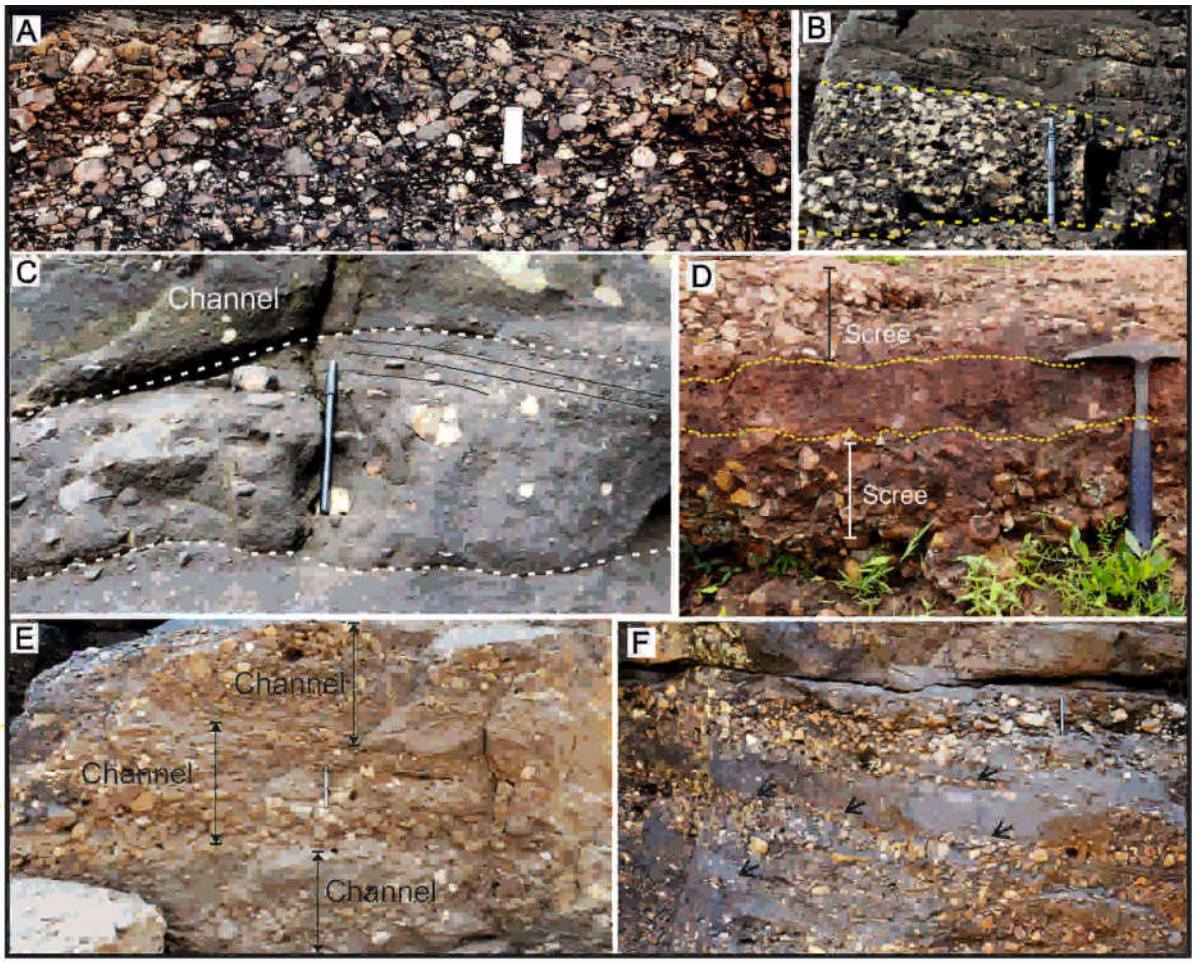

Figure 4

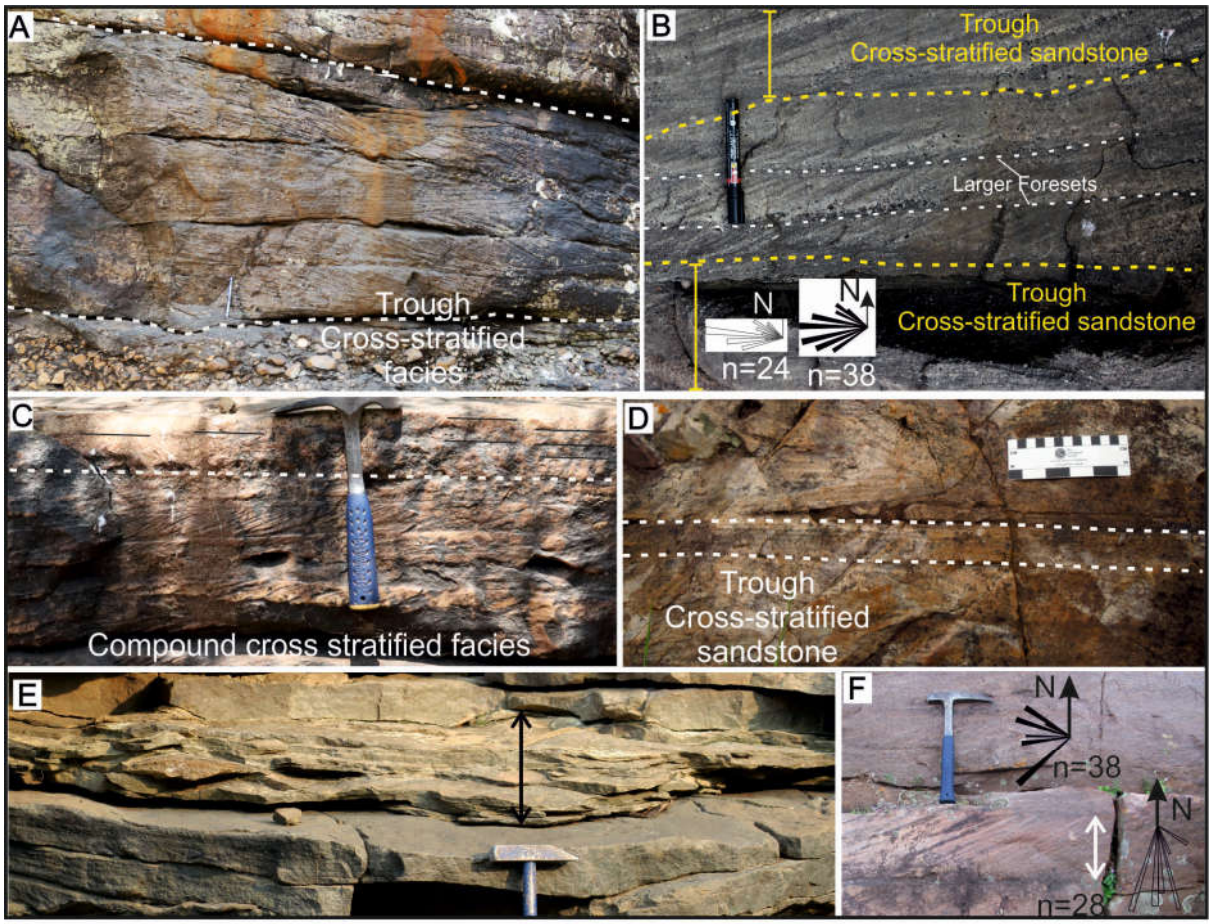
A
Trough
Cross-stratified
facies
B
Trough
Cross-stratified sandstone
Larger Foresets
N
n=24
N
n=38
Trough
Cross-stratified sandstone
C
Compound cross stratified facies
D
Trough
Cross-stratified
sandstone
E
F
N
n=38
N
n=28

Figure 5

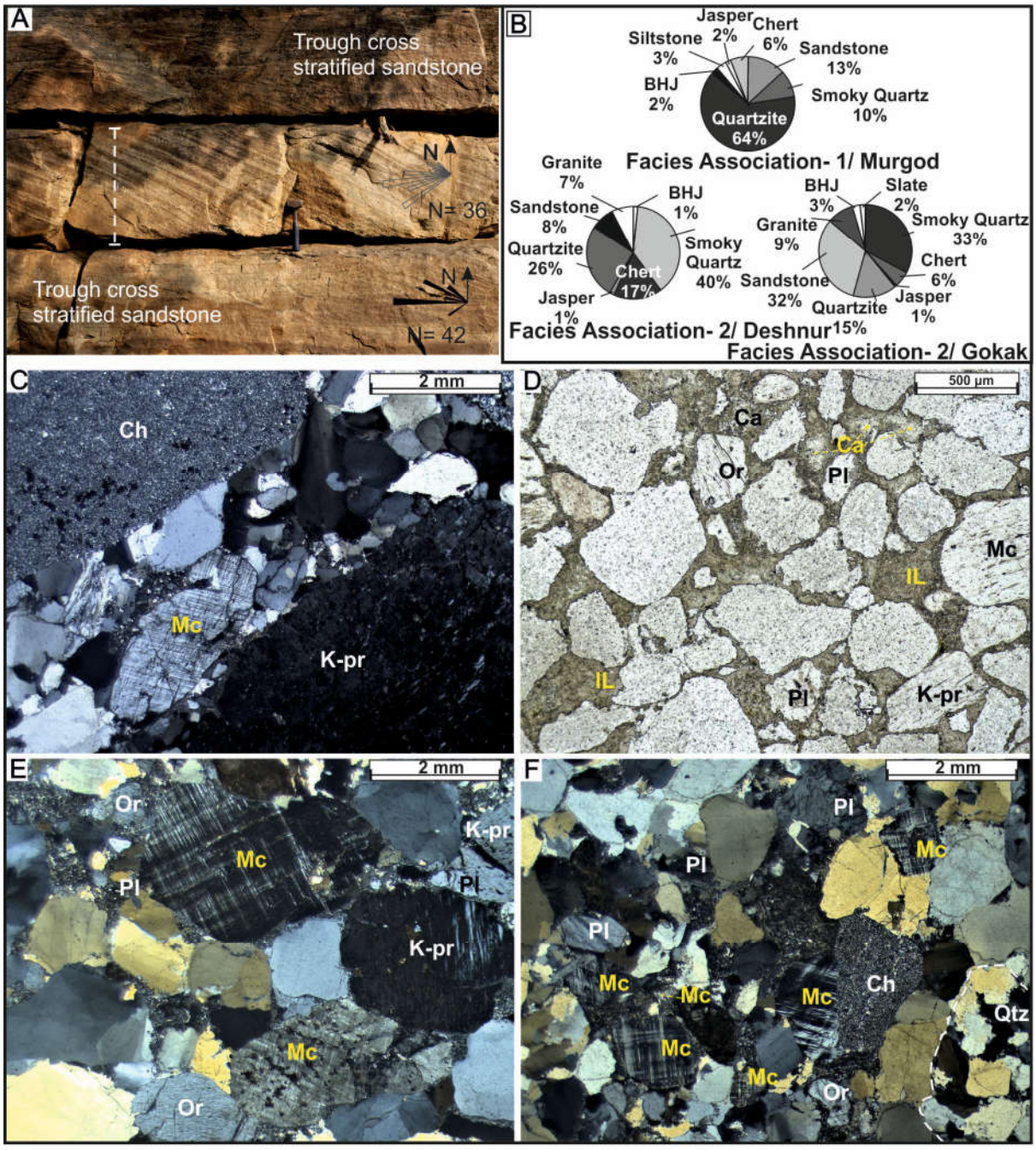
A
Trough cross stratified sandstone
N
N= 36
Trough cross stratified sandstone
N
N= 42
B
Jasper 2%
Chert 6%
Siltstone 3%
Sandstone 13%
BHJ 2%
Smoky Quartz 10%
Quartzite 64%
Facies Association- 1/ Murgod
Granite 7%
BHJ 1%
Sandstone 8%
Quartzite 26%
Smoky Quartz 40%
Chert 17%
Jasper 1%
Facies Association- 2/ Deshnur
BHJ 3%
Slate 2%
Granite 9%
Smoky Quartz 33%
Chert 6%
Sandstone 32%
Quartzite 15%
Jasper 1%
Facies Association- 2/ Gokak
C
2 mm
Ch
Mc
K-pr
D
500 µm
Ca
Ca
Or
Pl
Mc
IL
IL
Pl
K-pr
E
2 mm
Or
K-pr
Mc
Pl
Pl
K-pr
Mc
Or
F
2 mm
Pl
Mc
Pl
Pl
Mc
Mc
Mc
Ch
Qtz
Mc
Mc
Or

Figure 6

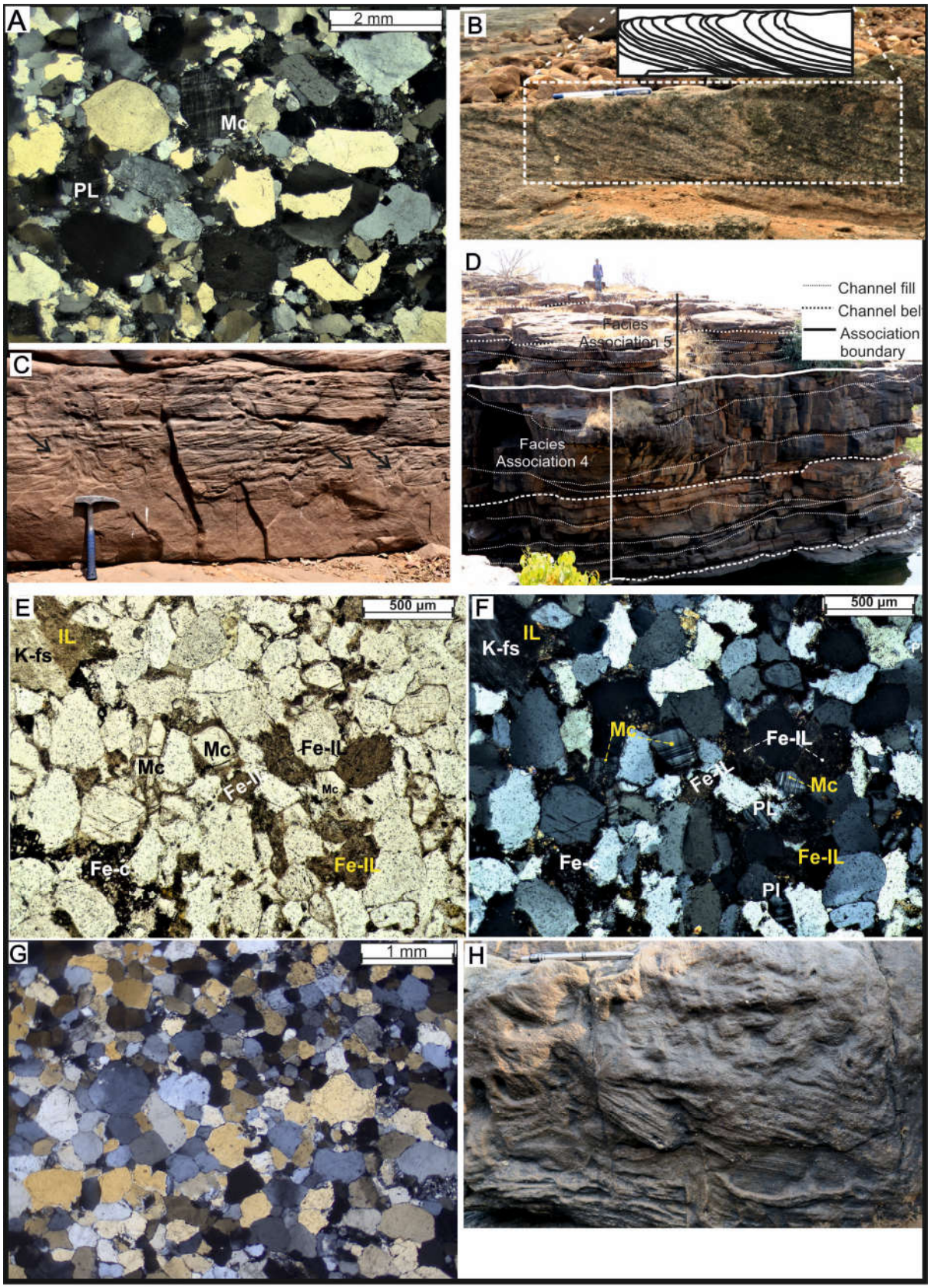
A
2 mm
Mc
PL
B
C
D
Channel fill
Channel bel
Association boundary
Facies Association 5
Facies Association 4
E
500 µm
IL
K-fs
Mc
Mc
Fe-IL
Fe-I
Mc
Fe-c
Fe-IL
F
500 µm
IL
K-fs
Mc
Fe-IL
Fe-IL
Mc
PL
Fe-IL
Pl
G
1 mm
H

Figure 7

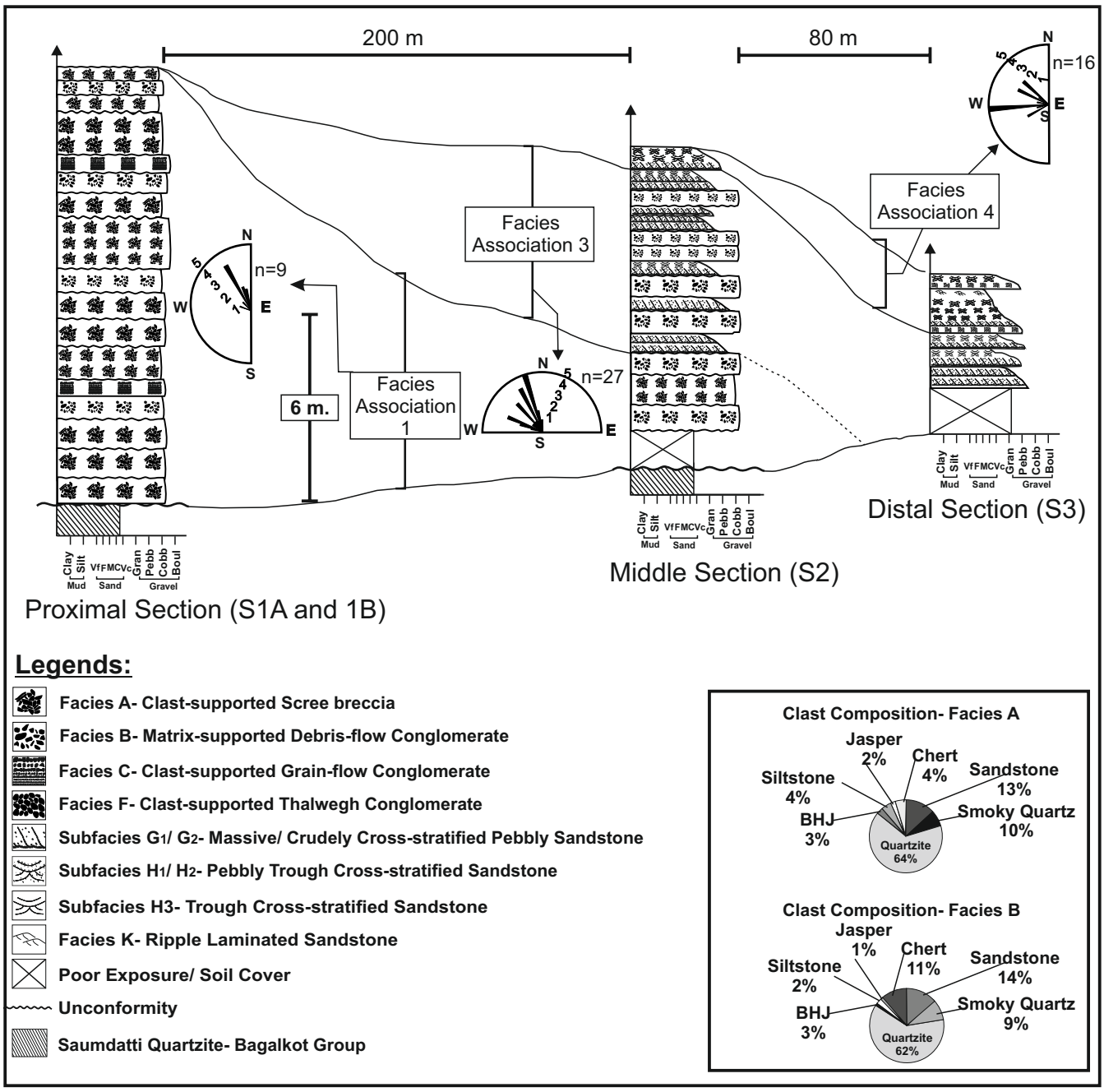
200 m
80 m
n=16
n=9
n=27
6 m.
Facies Association 1
Facies Association 3
Facies Association 4
Clay Mud
Silt
VfFMCVc Sand
Gran
Pebb
Cobb
Boul
Gravel
Proximal Section (S1A and 1B)
Middle Section (S2)
Distal Section (S3)
Legends:
Facies A- Clast-supported Scree breccia
Facies B- Matrix-supported Debris-flow Conglomerate
Facies C- Clast-supported Grain-flow Conglomerate
Facies F- Clast-supported Thalwegh Conglomerate
Subfacies G1/ G2- Massive/ Crudely Cross-stratified Pebbly Sandstone
Subfacies H1/ H2- Pebbly Trough Cross-stratified Sandstone
Subfacies H3- Trough Cross-stratified Sandstone
Facies K- Ripple Laminated Sandstone
Poor Exposure/ Soil Cover
Unconformity
Saumdatti Quartzite- Bagalkot Group
Clast Composition- Facies A
Jasper 2%
Chert 4%
Sandstone 13%
Smoky Quartz 10%
Siltstone 4%
BHJ 3%
Quartzite 64%
Clast Composition- Facies B
Jasper 1%
Chert 11%
Sandstone 14%
Smoky Quartz 9%
Siltstone 2%
BHJ 3%
Quartzite 62%

Figure 8

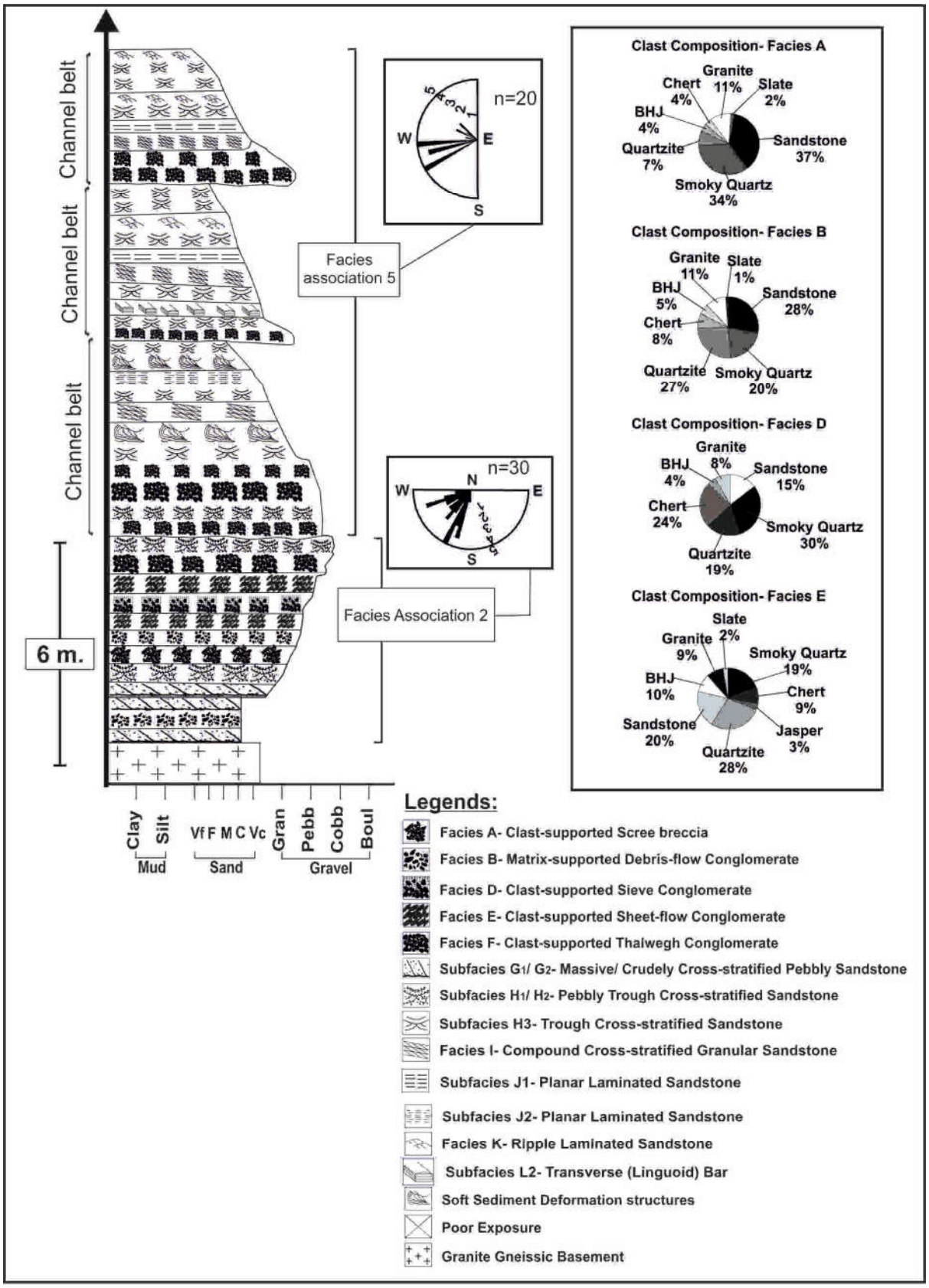
Channel belt
Channel belt
Channel belt
6 m.
n=20
W
E
S
Facies association 5
n=30
N
W
E
S
Facies Association 2
Clay
Silt
Mud
Vf F M C Vc
Sand
Gran
Pebb
Cobb
Boul
Gravel
Clast Composition- Facies A
Granite 11%
Chert 4%
Slate 2%
BHJ 4%
Quartzite 7%
Sandstone 37%
Smoky Quartz 34%
Clast Composition- Facies B
Granite 11%
Slate 1%
BHJ 5%
Sandstone 28%
Chert 8%
Quartzite 27%
Smoky Quartz 20%
Clast Composition- Facies D
Granite 8%
BHJ 4%
Sandstone 15%
Chert 24%
Smoky Quartz 30%
Quartzite 19%
Clast Composition- Facies E
Slate 2%
Granite 9%
Smoky Quartz 19%
BHJ 10%
Chert 9%
Sandstone 20%
Jasper 3%
Quartzite 28%
Legends:
Facies A- Clast-supported Scree breccia
Facies B- Matrix-supported Debris-flow Conglomerate
Facies D- Clast-supported Sieve Conglomerate
Facies E- Clast-supported Sheet-flow Conglomerate
Facies F- Clast-supported Thalwegh Conglomerate
Subfacies G1/ G2- Massive/ Crudely Cross-stratified Pebbly Sandstone
Subfacies H1/ H2- Pebbly Trough Cross-stratified Sandstone
Subfacies H3- Trough Cross-stratified Sandstone
Facies I- Compound Cross-stratified Granular Sandstone
Subfacies J1- Planar Laminated Sandstone
Subfacies J2- Planar Laminated Sandstone
Facies K- Ripple Laminated Sandstone
Subfacies L2- Transverse (Linguoid) Bar
Soft Sediment Deformation structures
Poor Exposure
Granite Gneissic Basement

Figure 9

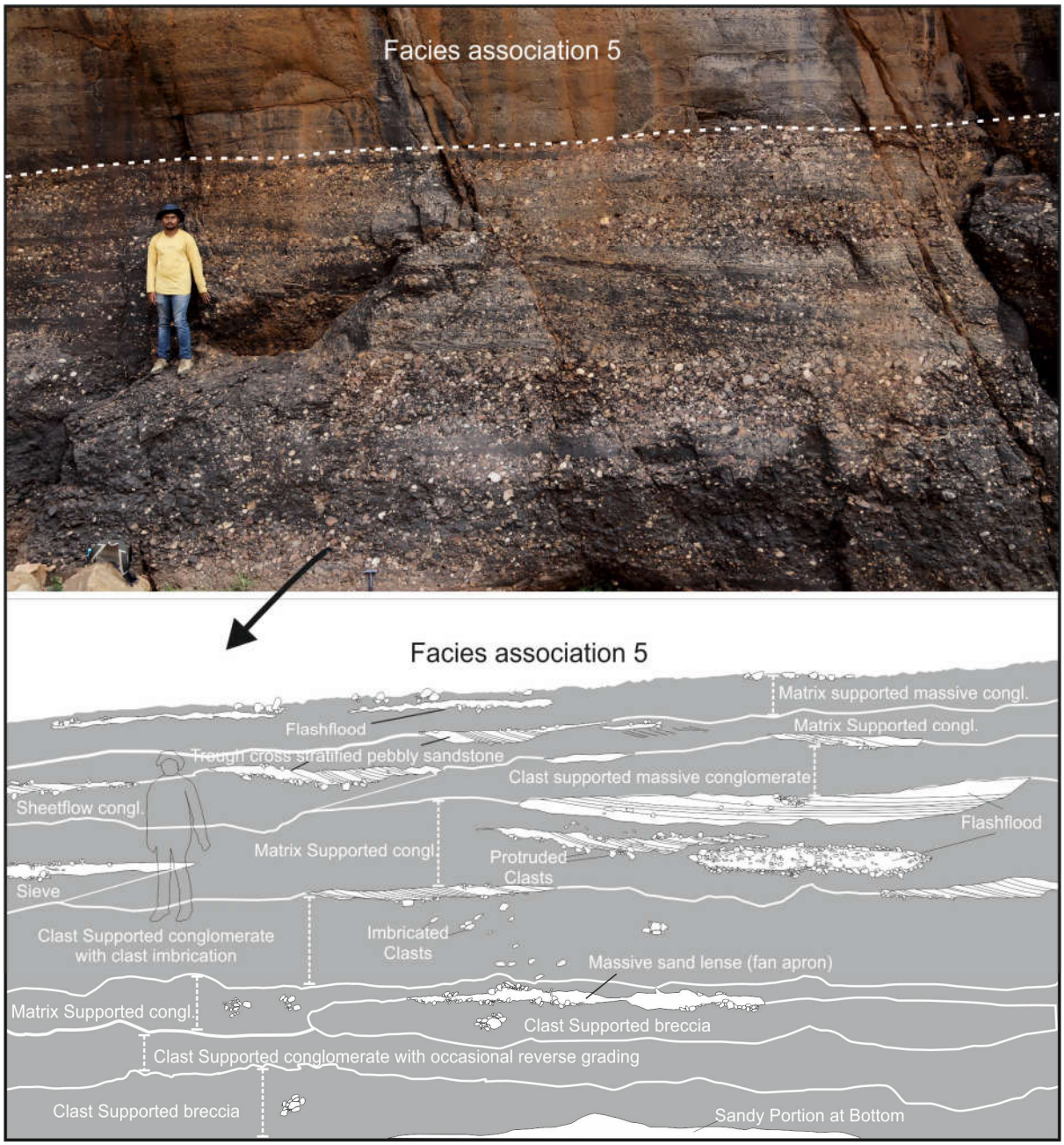
Facies association 5
Facies association 5
Matrix supported massive congl.
Flashflood
Matrix Supported congl.
Trough cross stratified pebbly sandstone
Clast supported massive conglomerate
Sheetflow congl.
Flashflood
Matrix Supported congl.
Protruded Clasts
Sieve
Clast Supported conglomerate with clast imbrication
Imbricated Clasts
Massive sand lense (fan apron)
Matrix Supported congl.
Clast Supported breccia
Clast Supported conglomerate with occasional reverse grading
Clast Supported breccia
Sandy Portion at Bottom

Figure 10

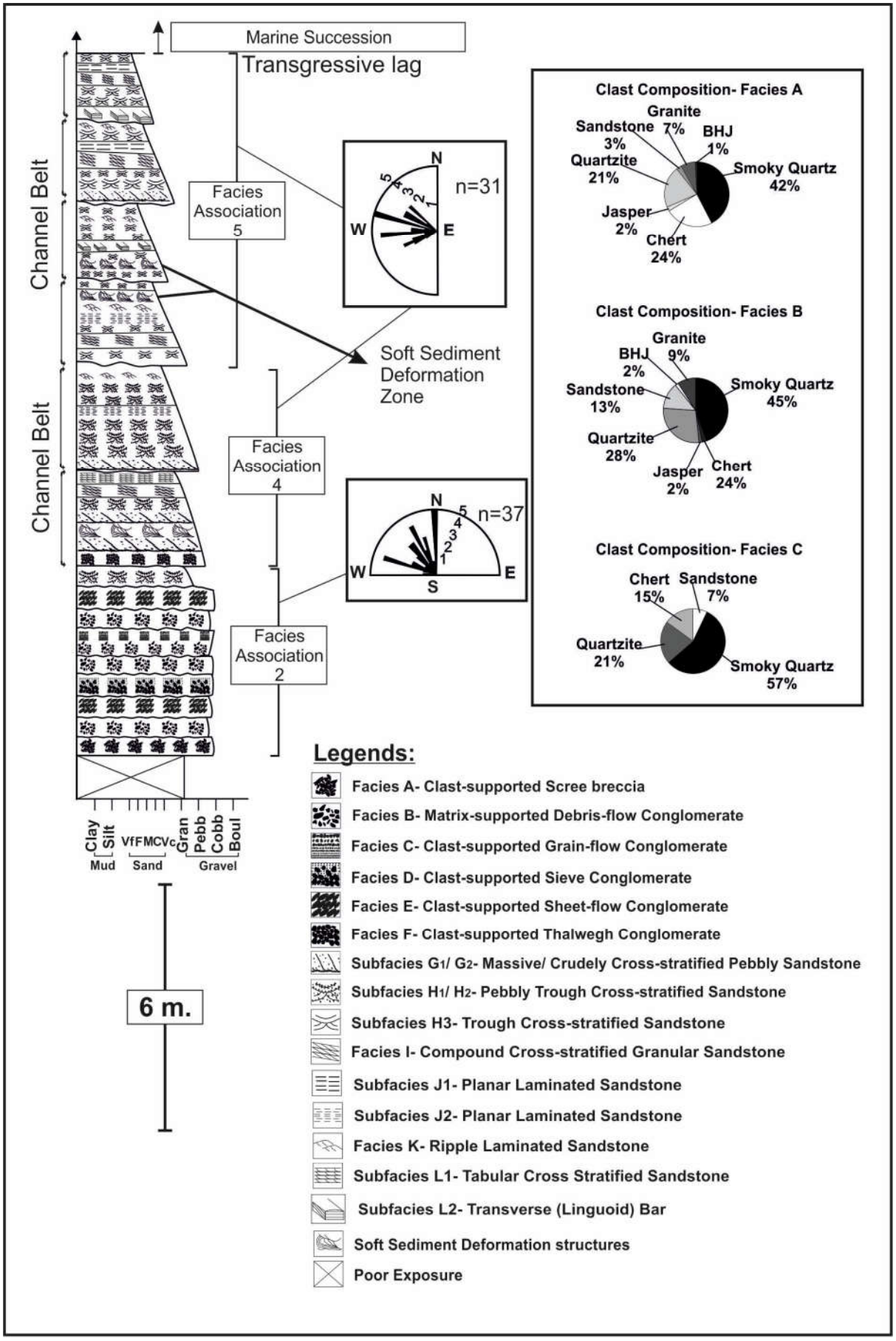
Marine Succession
Transgressive lag
Channel Belt
Channel Belt
Facies Association 5
Facies Association 4
Facies Association 2
Soft Sediment Deformation Zone
N
W
E
n=31
N
W
E
S
n=37
Clast Composition- Facies A
Granite 7%
Sandstone 3%
BHJ 1%
Quartzite 21%
Smoky Quartz 42%
Jasper 2%
Chert 24%
Clast Composition- Facies B
Granite 9%
BHJ 2%
Sandstone 13%
Smoky Quartz 45%
Quartzite 28%
Jasper 2%
Chert 24%
Clast Composition- Facies C
Chert 15%
Sandstone 7%
Quartzite 21%
Smoky Quartz 57%
Clay Silt VfFMCVc Gran Pebb Cobb Boul
Mud Sand Gravel
6 m.
Legends:
Facies A- Clast-supported Scree breccia
Facies B- Matrix-supported Debris-flow Conglomerate
Facies C- Clast-supported Grain-flow Conglomerate
Facies D- Clast-supported Sieve Conglomerate
Facies E- Clast-supported Sheet-flow Conglomerate
Facies F- Clast-supported Thalwegh Conglomerate
Subfacies G1/ G2- Massive/ Crudely Cross-stratified Pebbly Sandstone
Subfacies H1/ H2- Pebbly Trough Cross-stratified Sandstone
Subfacies H3- Trough Cross-stratified Sandstone
Facies I- Compound Cross-stratified Granular Sandstone
Subfacies J1- Planar Laminated Sandstone
Subfacies J2- Planar Laminated Sandstone
Facies K- Ripple Laminated Sandstone
Subfacies L1- Tabular Cross Stratified Sandstone
Subfacies L2- Transverse (Linguoid) Bar
Soft Sediment Deformation structures
Poor Exposure

Figure 11

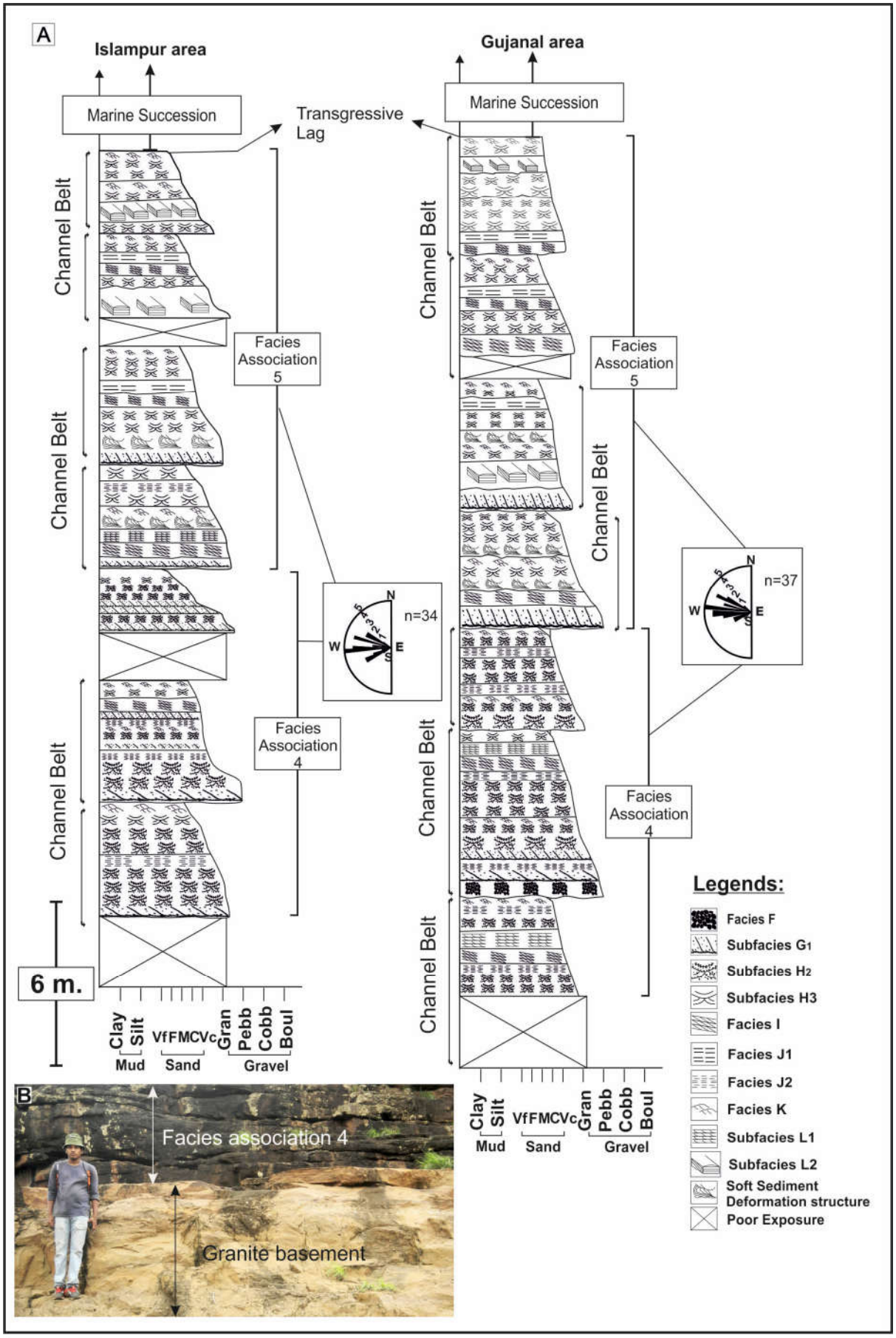
A
Islampur area
Gujanal area
Marine Succession
Marine Succession
Transgressive Lag
Channel Belt
Channel Belt
Channel Belt
Channel Belt
Channel Belt
Channel Belt
Facies Association 5
Facies Association 5
Facies Association 4
Facies Association 4
n=34
n=37
N
E
S
W
6 m.
Clay
Silt
Mud
VfFMCVc
Sand
Gran
Pebb
Cobb
Boul
Gravel
B
Facies association 4
Granite basement
Legends:
Facies F
Subfacies G1
Subfacies H2
Subfacies H3
Facies I
Facies J1
Facies J2
Facies K
Subfacies L1
Subfacies L2
Soft Sediment Deformation structure
Poor Exposure

Figure 12

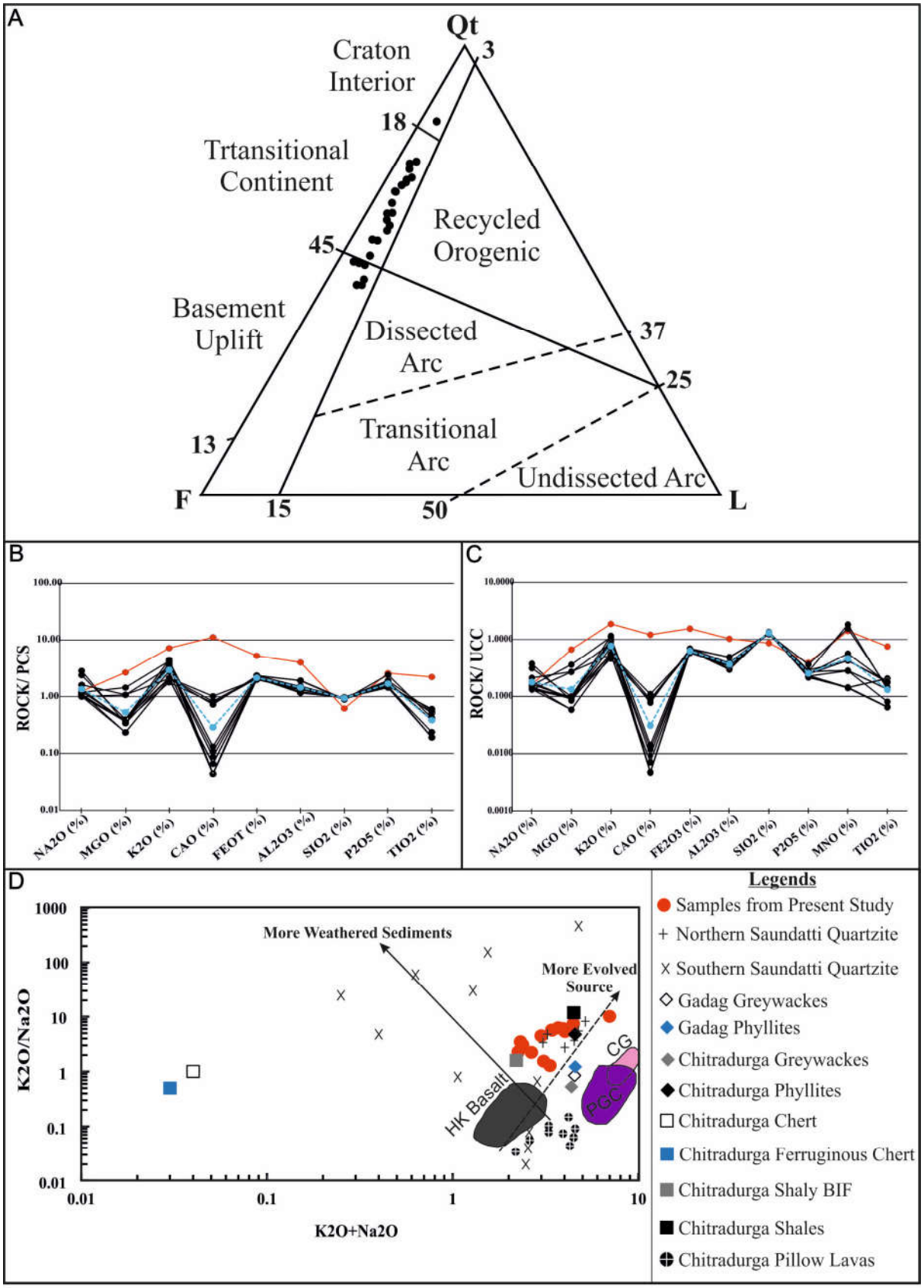
A
Qt
Craton Interior
3
18
Trtansitional Continent
Recycled Orogenic
45
Basement Uplift
Dissected Arc
37
25
Transitional Arc
13
Undissected Arc
F
15
50
L
B
ROCK/ PCS
100.00
10.00
1.00
0.10
0.01
NA2O (%)
MGO (%)
K2O (%)
CAO (%)
FEOT (%)
AL2O3 (%)
SIO2 (%)
P2O5 (%)
TIO2 (%)
C
ROCK/ UCC
10.0000
1.0000
0.1000
0.0100
0.0010
NA2O (%)
MGO (%)
K2O (%)
CAO (%)
FE2O3 (%)
AL2O3 (%)
SIO2 (%)
P2O5 (%)
MNO (%)
TIO2 (%)
D
K2O/Na2O
1000
100
10
1
0.1
0.01
0.01
0.1
1
10
K2O+Na2O
More Weathered Sediments
More Evolved Source
HK Basalt
CG
PGC
Legends
Samples from Present Study
Northern Saundatti Quartzite
Southern Saundatti Quartzite
Gadag Greywackes
Gadag Phyllites
Chitradurga Greywackes
Chitradurga Phyllites
Chitradurga Chert
Chitradurga Ferruginous Chert
Chitradurga Shaly BIF
Chitradurga Shales
Chitradurga Pillow Lavas

Figure 13

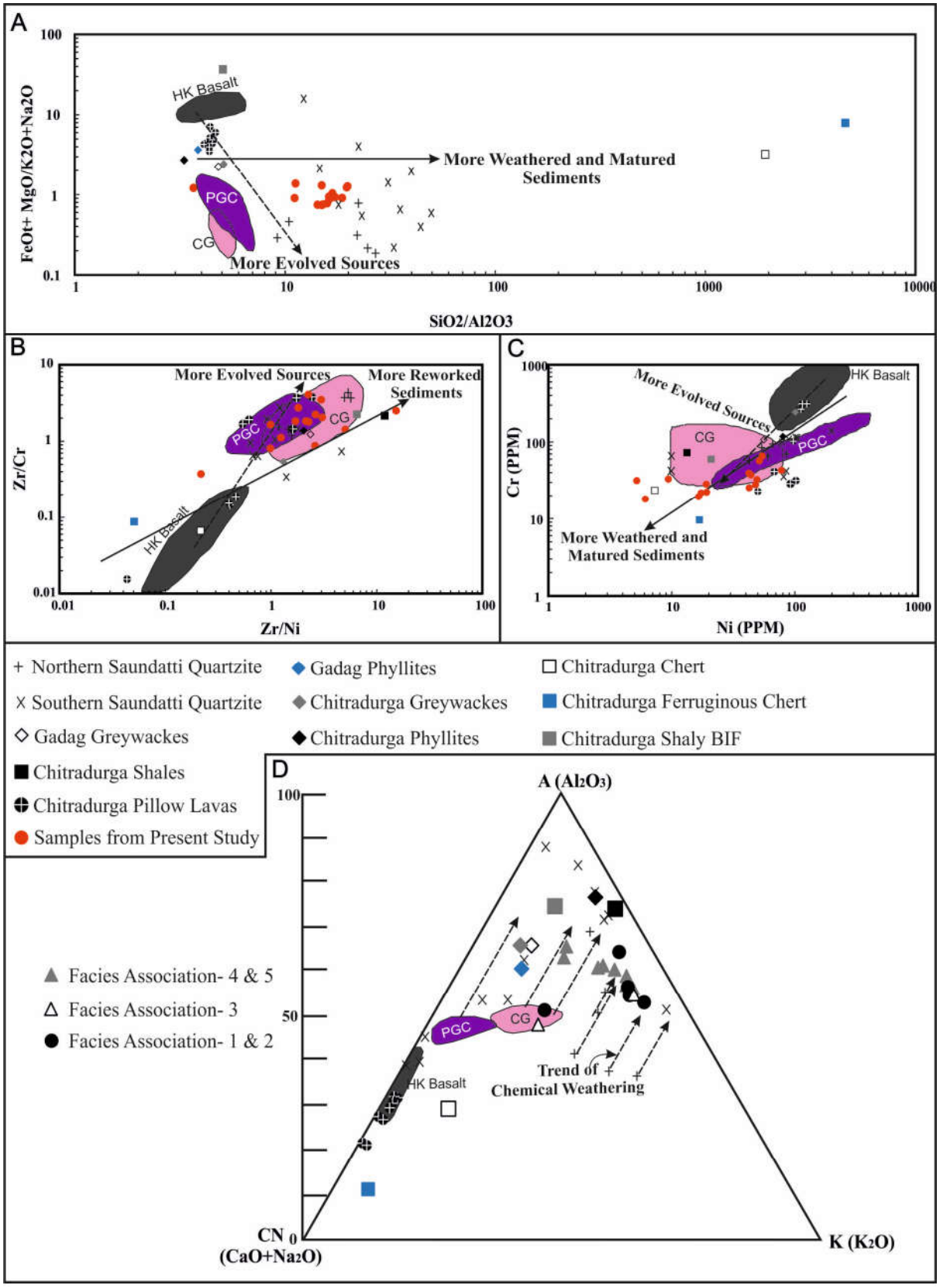
A
FeOt+ MgO/K2O+Na2O
SiO2/Al2O3
HK Basalt
PGC
CG
More Weathered and Matured Sediments
More Evolved Sources
B
Zr/Cr
Zr/Ni
More Evolved Sources
More Reworked Sediments
C
Cr (PPM)
Ni (PPM)
More Evolved Sources
More Weathered and Matured Sediments
+ Northern Saundatti Quartzite
X Southern Saundatti Quartzite
◇ Gadag Greywackes
■ Chitradurga Shales
⊕ Chitradurga Pillow Lavas
● Samples from Present Study
◆ Gadag Phyllites
◆ Chitradurga Greywackes
◆ Chitradurga Phyllites
□ Chitradurga Chert
■ Chitradurga Ferruginous Chert
■ Chitradurga Shaly BIF
▲ Facies Association- 4 & 5
△ Facies Association- 3
● Facies Association- 1 & 2
D
A (Al2O3)
CN (CaO+Na2O)
K (K2O)
Trend of Chemical Weathering

Figure 14

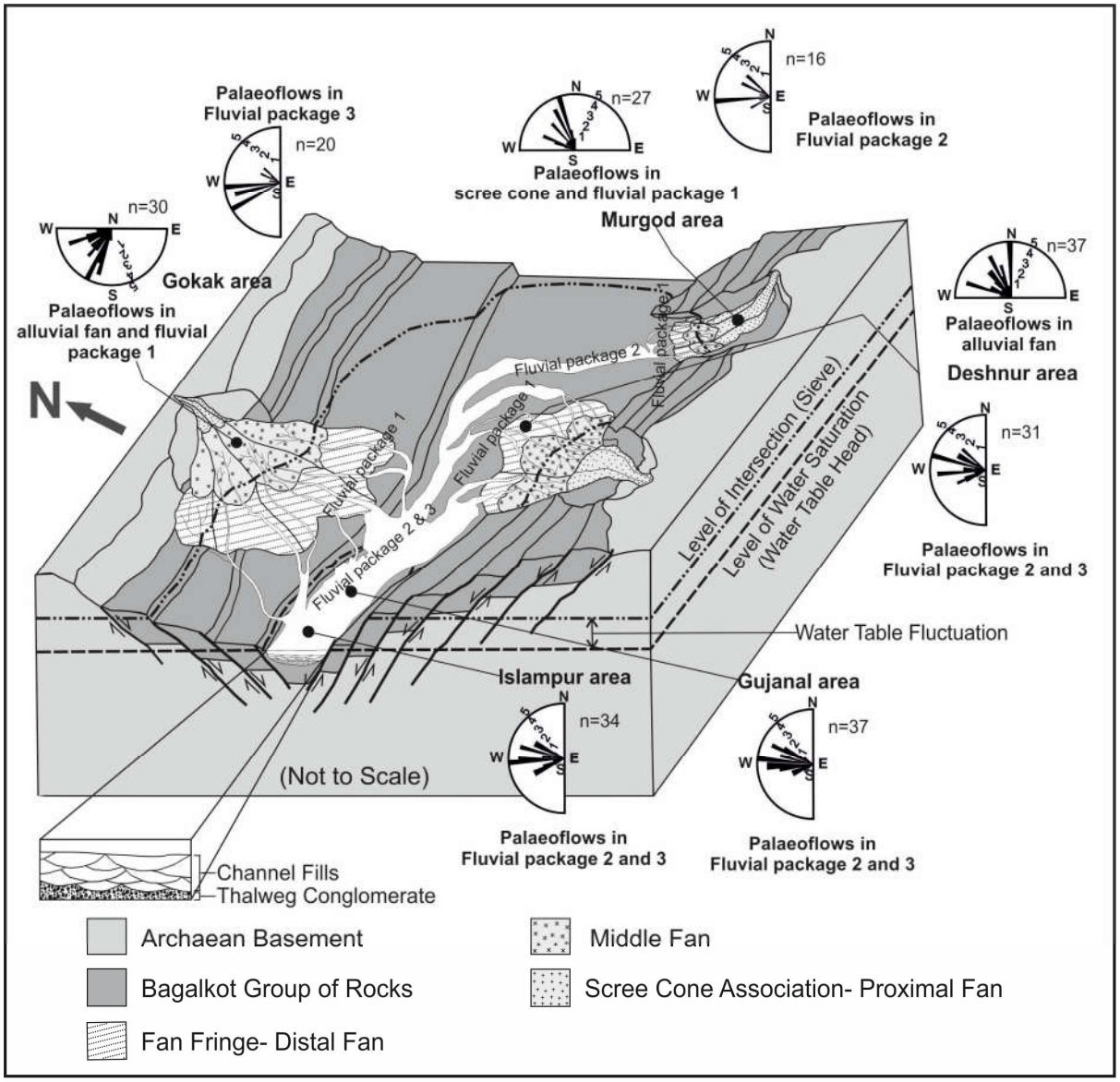
Palaeoflows in
Fluvial package 3
n=20
n=27
Palaeoflows in
scree cone and fluvial package 1
n=16
Palaeoflows in
Fluvial package 2
n=30
Gokak area
Palaeoflows in
alluvial fan and fluvial
package 1
Murgod area
n=37
Palaeoflows in
alluvial fan
Deshnur area
N
Fluvial package 1
Fluvial package 2
Fluvial package 2 & 3
Level of Intersection (Sieve)
Level of Water Saturation
(Water Table Head)
n=31
Palaeoflows in
Fluvial package 2 and 3
Water Table Fluctuation
Islampur area
Gujanal area
n=34
n=37
(Not to Scale)
Palaeoflows in
Fluvial package 2 and 3
Palaeoflows in
Fluvial package 2 and 3
Channel Fills
Thalweg Conglomerate
Archaean Basement
Middle Fan
Bagalkot Group of Rocks
Scree Cone Association- Proximal Fan
Fan Fringe- Distal Fan

Figure 15

Table 1: Sandstone and sandy matrix (with rare high mud content) of conglomerates representing facies association (location wise)

Sl No.	Sample Name	Type of Sample	Locality
1	BD-GK-2	Matrix of debris flow conglomerate- Facies Association 2	Gokak
2	BD-GK-3	TCS coarse grained Sst.- Facies Association 5 (Base of CB-1)	Gokak
3	BD-GK-1	Matrix of scree conglomerate- Facies Association 2	Gokak
4	BD-GK-10	TCS medium grained Sst.- Facies Association 5 (Top of CB-3)	Gokak
5	BD-GK-8	TCS coarse Sst.- Facies Association 5 (Middle of CB-3)	Gokak
6	BD-GK-7	Pebbly Sst.- Facies Association 5 (Base of CB-3)	Gokak
7	BD-GK-5	TCS coarse grained Sst.- Facies Association 5 (Base of CB-2)	Gokak
8	BG-DN-A-13	TCS medium grained Sst.- Facies Association 5 (Middle of CB-4)	Deshnur
9	BG-DN-A-12	TCS medium grained Sst.- Facies Association 5 (Bottom of CB-4)	Deshnur
10	BG-DN-A-14	TCS medium grained Sst.- Facies Association 5 (Top of CB-4)	Deshnur
11	BG-DN-A-11	TCS coarse grained Sst.- Facies Association 5 (Top of CB-3)	Deshnur
12	BG-DN-A-8	TCS coarse grained Sst.- Facies Association 5 (Base of CB-3)	Deshnur
13	BG-DN-A-7	TCS pebbly Sst.- Facies Association 4 (Middle of CB-2)	Deshnur
14	BG-DN-A-6	TCS pebbly Sst.- Facies Association 4 (Base of CB-2)	Deshnur
15	BG-DN-A-5	TCS pebbly Sst.- Facies Association 2	Deshnur
16	BG-DN-A-4	Massive pebbly Sst.- Facies Association 2	Deshnur
17	BD-MU-9	TCS coarse grained Sst.- Facies Association 3	Murgod
18	BD-MU-8	Massive streamlet pebbly Sst.- Facies Association 3	Murgod
19	BD-MU-7	Massive streamlet pebbly Sst.- Facies Association 3	Murgod
20	BD-MU-6	Matrix of debris flow conglomerate- Facies Associastion 1	Murgod
21	BD-MU-5	Matrix of debris flow conglomerate- Facies Associastion 1	Murgod
22	BD-MU-4	Matrix of scree conglomerate- Facies Associastion 1	Murgod
23	BD-MU-3	Matrix of scree conglomerate- Facies Associastion 1	Murgod
24	BD-MU-2	Matrix of scree conglomerate- Facies Associastion 1	Murgod
25	BG-DN-A-3	Matrix of scree conglomerate- Facies Association 2	Deshnur
26	BG-DN-A-2	Matrix of scree conglomerate- Facies Association 2	Deshnur
27	BG-DN-A-9	TCS medium grained Sst.- Facies Association 5 (Middle of CB-3)	Deshnur
28	BG-DN-A-10	TCS medium grained Sst.- Facies Association 5 (Top of CB-3)	Deshnur

Table 2: Point count modal percentage of minerals in sandstone and sandstone equivalent sandy matrix of conglomerates

Sl No.	Sample Name	Q_T		F	L	Matrix/ Clay content	Cement	Opaque & Heavy minerals	Recalc. To 100%			Classification
		Q_M	Q_P						Q_T	F	L	
1	BD-GK-3	54	5	29	4	7	0	2	65	**31**	**4**	Arkosic arenite
2	BD-GK-1	45	5	34	5	6	3	2	56	38	6	Arkosic arenite
3	BD-GK-10	61	6	22	3	4	2	3	73	24	3	Sub-arkosic arenite
4	BD-GK-8	61	4	22	3	7	0	3	72	24	4	Sub-arkosic arenite
5	BD-GK-7	57	5	25	4	6	3	1	69	28	4	Arkosic arenite
6	BD-GK-5	50	6	30	4	7	3	0	62	34	4	Arkosic arenite
7	BG-DN-A-13	57	7	24	4	6	2	0	70	26	4	Arkosic arenite
8	BG-DN-A-12	62	3	23	5	5	1	1	70	25	5	Arkosic arenite
9	BG-DN-A-14	74	5	13	3	3	2	0	83	14	4	Sub-arkosic arenite
10	BG-DN-A-11	65	4	20	4	6	0	1	74	22	4	Sub-arkosic arenite
11	BG-DN-A-8	51	3	31	6	7	2	1	60	34	6	Arkosic arenite
12	BG-DN-A-7	55	3	30	5	5	1	2	62	32	5	Arkosic arenite
13	BG-DN-A-6	52	5	32	5	5	0	2	61	34	5	Arkosic arenite
14	BG-DN-A-5	46	7	32	6	6	2	1	58	35	6	Arkosic arenite
15	BG-DN-A-4	40	6	40	5	7	0	1	51	44	6	Arkosic arenite
16	BD-MU-9	58	6	28	3	4	1	1	67	29	4	Arkosic arenite
17	BD-MU-8	34	9	41	7	5	3	1	48	45	7	Arkosic arenite
18	BD-MU-7	36	5	42	6	5	3	3	46	47	6	Arkosic arenite
19	BD-MU-4	39	5	39	3	7	5	1	51	45	4	Arkosic arenite
20	BD-MU-3	45	6	35	4	6	2	2	56	39	4	Arkosic arenite
21	BD-MU-2	38	8	37	5	6	5	2	53	42	6	Arkosic arenite
22	BG-DN-A-3	36	4	40	6	6	5	2	46	46	7	Arkosic arenite

23	BG-DN-A-2	37	9	41	4	5	2	2	51	45	4	Arkosic arenite
24	BG-DN-A-9	59	5	28	3	3	0	1	67	30	3	Arkosic arenite
25	BG-DN-A-10	61	4	25	4	4	0	2	69	26	5	Arkosic arenite

Table 3: Major (wt.%) and trace element (ppm) composition of analysed sandstone and sandstone equivalent sandy matrix of conglomerates.

Major oxides (wt%)																	
Sl No.	1	2	3	4	5	6	7	8	9	10	11	12	13	14	15		
Sample Name:	BD-GK-5	BD-GK-8	BD-GK-1	BD-MU-9	BD-GK-7	BG-DN-A-13	BG-DN-A-9	BG-DN-A-7	BG-DN-A-4	BD-MU-8	BD-MU-5	BD-MU-3	BG-DN-A-2	BD-GK-10	BG-DN-A-11	PCS	UCC
Location:	Gokak	Gokak	Gokak	Gokak	Gokak	Deshnur	Deshnur	Deshnur	Deshnur	Murgod	Murgod	Murgod	Deshnur	Gokak	Deshnur		
Na2O (%)	0.52	0.68	1.22	1.48	0.55	0.52	0.59	0.52	0.63	0.56	0.63	0.52	0.53	0.83	0.61	0.51	3.89
MgO (%)	0.21	0.20	0.22	0.19	0.20	0.13	0.13	0.21	0.21	0.20	1.48	0.60	0.22	0.60	0.80	0.55	2.20
K2O (%)	3.25	1.56	1.88	1.91	2.46	1.81	1.81	2.96	3.39	3.38	6.40	2.96	3.95	1.85	3.76	0.88	3.39
CaO (%)	0.02	0.35	0.46	0.38	0.02	0.03	0.03	0.05	0.02	0.02	5.11	0.04	0.02	0.33	0.06	0.45	4.19
Fe2O3 (%)	2.72	2.72	2.66	2.88	2.63	2.82	2.82	2.83	2.76	2.76	7.03	3.01	3.12	3.08	3.15	1.32	4.49
Al2O3 (%)	5.66	5.88	5.12	4.79	5.49	4.52	4.61	5.47	5.69	5.57	15.71	5.33	5.83	7.54	7.43	3.87	15.17
SiO2 (%)	89.62	87.70	88.33	89.34	88.70	89.52	90.36	88.65	85.02	84.14	57.47	89.32	83.07	84.41	82.35	92.15	65.89
P2O5 (%)	0.05	0.05	0.04	0.05	0.05	0.05	0.06	0.05	0.05	0.05	0.08	0.06	0.05	0.05	0.07	0.03	0.20
MnO (%)	0.01	0.01	0.01	0.02	0.01	0.02	0.02	0.04	0.01	0.01	0.10	0.03	0.03	0.13	0.11	0	0.07
TiO2 (%)	0.03	0.03	0.03	0.04	0.03	0.07	0.07	0.09	0.10	0.10	0.38	0.09	0.09	0.07	0.07	0.17	0.50
LOI	0.06	0.30	0.35	0.55	0.47	1.06	0.47	0.35	2.30	3.30	6.20	0.04	3.50	2.06	2.27	0	0.00
Total %	102.15	99.48	100.33	101.63	100.61	100.55	100.96	101.22	100.18	100.09	100.59	102.00	100.41	100.95	100.69	99.93	99.99
CIA	56.39	63.29	51.37	48.14	60.59	61.50	61.02	57.07	54.72	54.86	64.43	56.58	53.10	65.74	59.16	60.00	ND
CO2 %	ND	ND	ND	ND	ND	ND	ND	ND	ND	ND	3.66	ND	ND	ND	ND	ND	ND

Trace elements (ppm)																	
Sample Name:	BD-GK-5	BD-GK-8	BD-GK-1	BD-MU-9	BD-GK-7	BG-DN-A-13	BG-DN-A-9	BG-DN-A-7	BG-DN-A-4	BD-MU-8	BD-MU-5	BD-MU-3	BG-DN-A-2	BD-GK-10	BG-DN-A-11		
Rb (PPM)	94.40	96.70	112.20	112.20	94.70	9.70	11.70	9.70	122.50	107.70	23.00	86.80	112.20	9.70	12.33		
Sr (PPM)	43.30	41.60	67.20	67.20	37.50	11.40	14.20	30.40	41.60	38.10	32.70	36.70	67.20	25.20	33.45		
Ta (PPM)	2.70	2.30	2.10	2.10	2.60	3.00	2.20	2.40	5.40	2.30	1.20	2.30	2.10	2.20	2.56		
Th (PPM)	5.10	1.70	4.60	4.60	7.60	6.40	11.40	1.30	6.80	5.40	11.30	8.50	4.60	1.30	5.80		
U (PPM)	1.90	4.40	4.20	4.20	2.80	1.80	3.60	29.80	3.10	5.10	440.60	4.20	4.20	72.70	2.66		
V (PPM)	0.72	0.60	4.10	4.10	0.77	209.90	235.30	47.10	33.50	2.80	144.30	9.40	4.10	29.10	26.25		
Y (PPM)	22.20	20.00	20.50	20.50	19.80	20.40	24.70	21.60	20.70	25.60	32.40	23.40	20.50	23.70	22.65		
Ce (PPM)	21.50	20.00	32.60	32.60	18.40	10.20	29.60	40.20	35.40	23.70	35.30	30.40	32.60	25.80	27.06		
As (PPM)	17.60	18.50	19.25	19.66	13.70	14.50	13.80	0.01	17.70	18.30	0.02	19.20	19.43	12.80	13.60		
Ba (PPM)	295.72	298.94	498.47	511.20	305.43	171.10	165.41	418.25	321.44	285.90	475.62	355.37	504.82	334.33	377.51		
Cd (PPM)	19.30	17.10	0.30	0.30	21.30	1.90	2.10	4.90	0.32	0.30	0.90	0.30	0.30	0.30	0.27		
Co (PPM)	3.10	2.60	3.80	3.80	2.50	19.00	17.00	2.90	3.50	3.80	51.30	3.70	3.80	26.60	23.40		
Cr (PPM)	28.35	31.50	21.78	19.45	18.10	27.90	25.40	65.90	37.42	39.32	43.00	33.10	22.30	57.24	32.46		
Zr (PPM)	58.30	79.33	39.27	43.65	15.92	10.44	42.05	53.53	131.20	72.18	175.68	47.35	41.07	63.96	89.23		
Hf (PPM)	2.50	2.80	2.63	2.63	2.30	1.40	1.73	2.45	3.83	4.22	7.03	1.44	2.63	1.42	3.07		
Mo (PPM)	17.20	15.90	14.80	14.80	17.60	342.20	289.30	38.40	19.30	14.20	25.70	18.60	14.80	30.33	28.34		
Nb (PPM)	9.40	10.54	10.73	10.73	8.70	10.66	9.70	10.60	11.20	10.16	14.50	11.63	10.73	10.62	12.47		
Ni (PPM)	19.07	5.20	17.33	16.55	6.10	48.00	42.60	54.32	44.03	42.37	77.90	9.40	19.20	51.50	49.30		
Pb (PPM)	49.70	53.20	14.20	14.20	50.40	174.70	165.80	194.30	33.70	25.80	138.60	16.30	14.20	130.70	141.24		

Table 4: Facies constituents of the studied interval of the Badami Group

Facies	Description	Interpretation
Facies A. Clast-supported breccia	Characterized by clast supported breccia bodies (Fig. 3A), concentrating mainly towards the base of the stratigraphic sections; maximum thickness about 3.5 m; Casts are highly angular and very ill-sorted with matching boundaries of broken (Fig. 3B) and reclined clasts (Fig. 3A). Maximum clast sizes up to 70 cm. with an average of 18 cm; Strongly lenticular bodies with sharp and undulatory lower boundaries and less sharp upper boundaries; Clasts often penetrate into the lower substratum (Fig. 3C) as impinging clasts; Whenever found, wedge out rapidly away from the basin margin.	Interpreted as rock avalanche wedge or scree breccia facies (Shelley, 1965; Blair and McPherson, 1994).
Facies B. Matrix-supported conglomerate with protruded clasts	Composed of matrix supported, polymictic conglomerate bodies (Fig. 3D); Maximum clast size up to 30 cm; Chaotically arranged clasts are relatively smaller and less angular than the earlier facies; Bodies are lenticular with convex-up top and maximum thickness up to 1.4 m; Lower boundaries are planar while the upper boundaries are often undulatory because of frequent protrusion of clasts (Fig. 3D).	Interpreted as debris-flow conglomerate. Chaotic arrangements and protrusion of clasts indicates high matrix strength of the flows (Smith, 1986).
Facies C. Clast supported conglomerate with reverse grading	Characterized by clast supported conglomerate bodies with occasional reverse grading of clasts (Fig. 3E). Clast size is comparatively smaller than the preceding facies with maximum clast size is around 18 cm; Commonly associated with facies B.	Interpreted as modified grain-flow facies (Middleton, 1970; Lowe, 1976; Davis *et al*., 2002; Mahanta *et al*., 2019). The reverse grading of clasts indicating dispersive pressure (Pettijohn, 1975).
Facies D. Clast supported conglomerate grading upward into sandstone	Composed of clast supported conglomerate at the base giving rise to sandstone towards top; Bodies are discernibly convex-up and the sandy top part contains occasional cross strata; Sand grains appear to infiltrate within the larger clasts from top (Fig. 3F). Maximum thickness is about 55 cm and outcrop length is generally less than 3 m.	Inferred to be of sieve origin (Wasson, 1974; Milana, 2010 and references therein); Convex-up nature and progressive increment of sand towards top indicates bedforms were frozen due to rapid draining out of water, thereby resulting into infiltration of sand from top (Wasson, 1974).
Facies E. Clast	Composed of clast supported conglomerate with sheet-like body	Interpreted as sheet flow facies (Fisher, 1971; Blair and

supported conglomerate with clast imbrication	geometries; Thicknesses of individual bodies varies within 30 to 50 cm; Clasts are comparatively more rounded and show either bed-parallel or slightly imbricated alignment with their intermediate axis (Fig. 4A); Generally associated with facies D and occasionally with facies B.	McPherson, 1994); Sheet-like body geometry and clast supported nature with imbrication of intermediate axis indicate deposition from high flow regime tractive current (Walker, 1984).
Facies F. Clast supported massive conglomerate	Characterized by clast supported, massive lenticular conglomerate bodies, erosional bases and flat tops (Fig. 4B); Clasts are comparatively smaller in size (average size 2.7 cm) as well as more rounded; Followed upward invariably by thoroughly trough cross-stratified sandstone bodies (Fig. 4B); Occasionally, a crude normal grading, among the clasts can be observed.	Clasts almost certainly moved as rolling or sliding load; Rounding of the clasts can be attributed to abrasion during transport as bedload; Close association with thoroughly trough cross-stratified sandstone facies along with the typical geometry pointed towards their origin as the product of highest fluid gravity flow within a channel; Such conglomeratic bodies are likely to be the channel thalweg deposits, designated as channel lags by Allen (1982).
Facies G. Very coarse grained massive sandstone	Composed of very coarse grained, often pebbly, sandstone bodies, internally massive, with occasional crudely developed cross-strata to planar laminae towards top; Two distinct subfacies depending upon the body geometry and association; Dominant one (subfacies G_1) strongly lenticular body geometry with sharp bases and convex-up and less sharp tops (Fig. 4C); Very poor sorting with oversized pebbles, ranging in size from 5 mm to 20 mm, floating within the very coarse to coarse grained sandstone; Very rare but, whenever found, are associated with thoroughly trough cross-stratified sandstone facies; Other subfacies (G_2) constitute even lesser portion of the succession and is restricted to Murgod and Gokak area only; Characterized by thin (less than 15 cm in thickness), broadly lenticular bodies and is always associated with scree breccia facies (facies A, Figs. 3A, C, 4D); Outcrop length rarely exceeds 32 cm; Evidence of erosion is generally lacking at their bases; Oversized pebbles are rare; Sometimes	Coarse grain-size and massive nature along with their scarcity in occurrence indicate their high flow regime origin for both the subfacies; Subfacies (G_1) with oversized pebbles is possibly of high-velocity flashflood origin (Pfluger and Seilacher, 1991); Lenticular body geometry indicates channelised flow; Subfacies (G_2) indicates deposition on steep slopes from high energy flows, inferred from the close association with the scree bodies; Palaeocurrent directions, although not very informative because of rarity of data, probably represent local slope; Represent hill-slope deposit, formed due to the occasional flow of rain water over steep scree cone slopes; Considered to be of fan apron origin; Gradational transition from massive to cross bedding reflects decreasing flow strength,

	bear crude cross bedding to planar lamination; Petrographically as well as in appearances, these sandstone bodies are similar to the matrix present within Facies A; Palaeocurrent directions derived from crude cross stratification (though rare) show ample variability, however, consistent in each section.	while planar laminae towards top indicates increase in flow shear with decrease in flow depth; Similar to hillwash facies described by Bose *et al*. (2008).
Facies H. Trough cross stratified sandstone	Characterized by poorly sorted lenticular sandstone bodies in transverse sections; Concave-up erosional bases and sharp but flat tops; Internally thoroughly trough cross stratified; Coset and set thicknesses decreasing upward within individual unit as well as up the stratigraphic section; Appears to be the most dominant facies of the studied stratigraphic interval; Three distinct subfacies can be established depending upon the grain; First subfacies (H_1) is pebbly to coarse sand-sized with profuse oversized pebbles, the other two lacks them (Fig. 4E); Oversized pebbles are usually distributed randomly within the bodies, although concentration of comparatively smaller pebbles is discernible along the channel bases as well as coset or set boundaries; Locally this subfacies shows some strongly lenticular bodies with crudely developed trough cross stratification; Second subfacies (H_2) is very coarse to medium grained sandstone, with rare pebbles, concentrating along the bases (Fig. 4F); Third subfacies (H_3) is completely devoid of any pebbles and is made up of coarse to fine sand-sized sediments (Fig. 5A). Apart from the decreasing mean grain-size, grains are texturally more matured from first to third subfacies; Gradual decrease in grain-size, irrespective of subfacies, can be discernible along each unit as well as up the succession; Location specific unimodal palaeocurrent direction can be ascertained.	Poorly sorted sandstone with channelform geometry clearly suggests fluvial channel origin; Produced by dune migration along the channel floor under tractive current (Miall, 1985; Samanta *et al*, 2016). Gradual decrease in grain size, set and coset thickness within individual unit clearly suggest flow weakening. Decreasing grain size as well as increasing textural maturity from first to third subfacies pointed towards gradually increasing distance from the source (Pettijohn, 1975). Local subfacies H_1 with crude cross strata and randomly distributed oversized pebbles indicate product of rapid deposition from heavily loaded flow, possibly of flash flood origin (e.g., Pflüger and Seilacher, 1991; Sarkar *et al*, 2012); Presence of oversized pebbles, in general, points towards flow fluctuations within channels (Frostick and Reid, 1989; Mazumder and Sarkar, 2004; Mukhopadhyay *et al*., 2019).
Facies I. Compound cross stratified	Composed of poorly sorted lenticular sandstone in transverse sections, having flat bases and convex-up tops; Internally compound cross-stratified, with both the	Poorly sorted sandstone with unimodal palaeocurrent indicate fluvial origin; Large solitary trough cross set represents core,

sandstone	larger as well as smaller foresets dipping in the same direction (Fig. 5B); Occasionally some large solitary set of trough cross strata is observed below or upcurrent to the compound cross-stratified units; Pebbles, whenever present, are mostly concentrated along the larger foresets of the compound cross strata; Mostly found to be associated with the trough cross stratified facies, having slightly coarser grain size than the associated facies; Palaeocurrent data, from both the larger as well as smaller foresets, appear to be consistent, location-wise, with the direction derived from the associated trough cross stratified unit.	compound cross-strata represents the accretionary part of bar (Collinson and Thompson, 1989; Collinson, 1996; Mazumder and Sarkar, 2004); Compound cross-strata having same orientation of larger and smaller foresets indicates migration of bar along channel floor (Collinson and Thompson, 1989, Smith and Rogers, 1999; Best *et al*., 2003; Bridge, 2003; Miall and Jones, 2003; Eriksson *et al*., 2006b).
Facies J. Planar laminated sandstone	Characterized by tabular sandstone bodies, internally planar laminated; Restricted in occurrence; Two distinct subfacies; First subfacies (J_1) overlies the compound cross-stratified facies with sharp contact (Fig. 5C); Constituting grains are comparatively well rounded and preferably made up of the coarsest fraction of the underlying unit; Thin layers of pebble concentration on bedding surfaces locally; Second subfacies (J_2) overlies the trough cross-stratified facies with sharp contact, without any discernible change in grain size (Fig. 5D); Former variety is thinner (not exceeding 15 cm thickness) and laterally impersistent, the latter shows considerable thickness.	Internal planar laminae in reference to sediment grain size, indicate high flow regime (Miall, 1996); First variety produced by high energy shooting flows during falling water stage (Cant, 1978; Miall, 1996; Bridge, 2003; Hassan, 2005); Local pebble concentration indicates sediment winnowing owing to exposures of bar top (Cant, 1978; Kirk, 1983; Bridge, 2003); Second variety indicates shooting flow due to increasing flow shear resulting from fall of water level at the penultimate stage of filling (Harms *et al*., 1975).
Facies K. Ripple laminated sandstone	Characterized by broadly lenticular but impersistent sandstone bodies, internally ripple laminated (Fig. 5E), but, whenever found, almost always overlie the trough cross-stratified facies with sharp but non-erosional contact.	Product of ripple migration on channel floor under lower flow-regime (Harms and Fahnestock, 1965; Simons *et al*., 1965); Decreasing in-channel depth and velocity of water result smaller scale ripples replacing larger dunes (Harms *et al*., 1975).
Facies L. Tabular cross stratified sandstone	Characterized by tabular cross stratified lenticular sandstone bodies with sharp and planar upper and lower boundaries; Two subfacies recognized; Subfacies L_1, restricted in occurrences and always associated closely with compound trough cross stratified facies (Fig. 5F), reclining	Tabular cross-strata indicates avalanching of sediments along the steeper-side bars under the influence of current (Blatt *et al*., 1980; Collinson and Thompson, 1989); L_1 with reclining nature with strongly lenticular geometry

	over it; Strongly lenticular (rarely exceeding 50 cm outcrop length) and thicknesses never exceeds 30 cm; Foreset dip direction is at high angle to the general palaeocurrent direction, derived from associated trough and compound cross strata (Fig. 5F); Other subfacies L_2, with large tabular cross strata, often exceeding 50 cm in thickness (Fig. 6A), relatively dominant in occurrence, however, confined to a particular stratigraphic interval; Consistent palaeocurrent directions conforming the flow directions of channel troughs and compound cross strata (Fig. 6A).	and high angle palaeocurrent direction, inferred its origin by the collapse of bar top along the flanks (Long, 2004, 2011); Possibly formed during low water stage by secondary flow operated at high angle to the bar axes (Long, 2004, 2011); L_2 with similar palaeocurrent direction with channels troughs points towards transverse bar origin (Sarkar *et al*., 2012).

Table 5: Facies association and their inferred palaeogeography

Facies association	Inferred palaeogeography
1: Characterized by coarsest fraction of sediments represented by disordered breccia and conglomerate bodies; Rapidly wedging and having restricted clast compositions traceable into the adjacent basements (Fig. 6B); Major facies include scree (A) and debris flow (B), with minor modified grainflow (C); Fan apron subfacies (G_2), few other minor constituents are exclusive; Scree breccia bodies rapidly wedging downslope, are most dominant facies and are thicker and coarser than other constituent facies; Amalgamations of sediment gravity flow products are common, occasional intercalation of thin subfacies G_2 bodies; Clast-supported conglomerates are mostly feldspar-rich, poorly sorted matrix having very coarse to coarse sand sized angular to sub angular grains (Fig. 6C) with rare dominance of clay-sized particles; Matrix of the debris flow conglomerates (facies B) shows greater amount of clay minerals like sericite, chlorite, illite or ferric illite (Fig. 6D), rare occurrence of ferruginous and calcitic cement in few samples of facies A and B (Fig. 6D); Restricted in occurrence, almost always overlies the basement and occupies most proximal position of the basin margin.	Coarsest grain size pointed towards super-proximal palaeogeography; Dominance of scree bodies, with occasional debris flow and grain flow indicates deposition from highly sediment-laden flows moving along a high slope; Scree bodies pointed towards free fall of rock mass along high slopes of basin margin in periods of tectonic unrests; Presence of debris-flow and other sediment gravity flow reflects high density, coarse grained, viscous flows, induced by heavy rains; Rare presence of fan apron sandstone bodies indicates relatively low density flows generated along the steep hillslopes during occasional rains; Feldspar rich, coarse sandy matrix also supports short transportation and quick burial, derived from a tectonically active provenance; Super proximal position with dominance of rapidly wedging scree bodies, indicate screecone palaeogeography.
2: Characterized by conglomerates of both sediment gravity flow and fluid gravity flow origin, along with secondary sandstones and rare breccia bodies; Overall coarsening upward stratigraphic trend with sandy lower portion and conglomeratic upper portion; Clast composition of rudaceous sediments show wider spectrum than earlier association (Fig. 6B), though the matrix is similar in composition, the grain size is comparatively finer and ranges from coarse to medium sand, sub-angular to sub-rounded; Major facies constituents include debris flow (B), sheet flow (E), sieve (D), channel thalweg (F) and channelform subfacies (H_1) with subordinate scree (A), modified grainflow (C) and flashflood subfacies (G_1); Rare hillwash subfacies (G_2) over scree bodies; Lower part dominated by medium grained trough cross	Dominance of coarse-grained mass-flow deposits with discernible coarsening upward trend indicates prodrading alluvial fan in semi-arid climatic condition (Middleton and Hampton, 1973, 1976; Lowe, 1979; Nemec and Steel, 1984; Rust and Koster, 1984; Nilsen, 1985; Blair and McPherson, 1994); Upper fan dominated by debris flows, middle fan characterized by sheet flows and sieve deposits, lower fan dominated by channel sandstone and flashflood deposits; Channelized pebbly sandstone characterized the basal part of the lower fan indicates deposition below intersection point between fan surface with water table (Hooke, 1967; Wasson, 1974). Overlying sheet flow and sieve deposits typically represents middle fan,

stratified sandstone bodies (subfacies H_1) with occasional thalweg conglomerates (F) and flashfloods (G_1); Rare sieve deposits (D) and sheet flow conglomerates (E) also present; Middle part mostly rudaceous with sheet flows (E) and sieve deposits (D), intercalated with infrequent scree (A) and coarse grained trough cross-stratified sandstone bodies (H_1); The upper part dominated by debris flow (B) and scree (A) with rare modified grainflows (C); Petrographically, the arenaceous fractions are arkosic, with angular to subangular coarse grained having moderate to poor sorting (Fig. 6E).	near the intersection point; However, sieve deposits are typically occurred in the proximal or middle to lower fan areas with sheetflow during early stage of fan growth depending on fan development stage (Blair and McPherson, 1994); Association of sieve with both middle to distal fan suggest seasonal or higher scale water table fluctuation (Mukhopadhyay, 2012); Overlying debris flow dominated part accounts for upper fan, occurred above the intersection point; Occurrence of scree breccia at different level indicates basement uplift thereby influencing basin filling. Proximal position supported by textural attributes.
3: Typified by channel-fill pebbly sandstone; Major facies constituents include pebbly to coarse sand-sized thoroughly trough cross-stratified with oversized pebbles, laterally and vertically juxtaposed, facies (H_1) (Fig. 4E), with subordinate channel thalweg facies (F), planar laminated (J_2) and flashflood (G_1) subfacies and rare ripple laminated (K) facies; Channelform subfacies (H_1) is dominantly underlain by thalweg facies at basal part (Fig. 4B); Planar laminated subfacies (J_2) frequently overlies the channelform subfacies, towards top (Fig. 5D); Ripple laminated facies, whenever present always follows channelform subfacies (Fig. 5E); Flashflood bodies are frequently present within the lower part; Lithologically, the sandstone bodies are arkosic to subarkosic arenite, with significant feldspar content and high textural immaturity (Fig. 6F); Gradual grain-size reduction up-the-succession.	Dominance of in-channel trough cross-stratified facies makes fluvial origin apparent (Miall, 1981); Initial conglomeratic facies represents highest flow velocity product; Presence of oversized pebbles within channels pointed towards flow instability (Pfluger and Seilacher, 1991); Upward transition from low to high flow regime channel-fills structures indicates ephemeral nature of the streamlets (Olsen, 1989; Mukhopadhyay *et al*., 2014); Presence of occasional flashfloods attests the contention further (Pfluger and Seilacher, 1991). Palaeogeography appears to be steeper slope area, not far away from the basin margin; Frequent vertical and lateral juxtaposition of channelform sandstone bodies pointed deposition from high gradient, rapidly avulsive streamlets (Bose *et al*., 2008). Arkosic nature and textural immaturity of the sandstone supports less transportation and rapid deposition.
4: Characterized by tabular to broadly lenticular storeys of vertically stacked sandstone body; Maximum thickness of each storey never exceeds 7 m; Longitudinal bar (I) and channelform subfacies (H_2) are most common constituents, although ripple laminated (K), planar laminated (J), tabular cross-stratified (L_1) and massive pebbly sandstone (G_1) facies are also present in	Abundance of mid-channel bars point to braided nature of the river channels (Miall, 1988); Occurrences of frequent scourings at the base of storey point towards inconsistency of flow; Sheet sandstone over both channelform and barform deposits indicates fall of water level, even emergence of the barform suggesting flow fluctuations (Olsen,

successively lesser amount; Each storey is made up of lateral and vertical juxtaposition of channelforms (H_2) and barforms (I), showing onlapping/downlapping relationship, with infrequent sheet flows (J_1 and J_2) and ripple laminations (K); While sheet flows are more common in basal storeys, ripple migration appears in upper ones; Tabular cross stratified (L_1) and massive pebbly sandstone (G_1) bodies are rare; Mid-channel positions of the longitudinal barforms are discernible locally; Constituent sandstone bodies are coarse to medium sand-sized, with rare pebbles (or granules), and texturally more matured than the sandstones of previous associations; Pebbles or granules, whenever present, tend to concentrate along the erosional bases of the storeys; Lithologically such sandstone bodies are dominantly subarkosic arenite (Fig. 7A) with feldspar grains altered partially or thoroughly to sericitic or illitic minerals.	1989; Miall, 2014), supported by rare presence of flashflood deposits; Infrequent occurrences of deformed and overturned cross strata further supports high energy flashy nature of the flows (Fig. 7B, C; Picard and High, 1973; Frostick and Reid, 1977; Tunbridge, 1981, 1984; Olsen, 1987; Dam and Andreasen, 1990; Long, 2004; Mukhopadhyay *et al*, 2014). Comparatively finer and relatively matured nature of the sediments, with lesser amount of oversized pebbles, indicates lesser extent flow fluctuations; Fluvial deposition apparently took place on plain land beyond the basin marginal influence; Subarkosic nature of the constituent sandstone bodies further supports the connotation. Altered feldspar grains suggests increased chemical weathering rate.
5: Composed of storeys of sheet like sandstone body, and are thinner (<4 m) than the storeys of earlier associations (Fig. 7D); Pebbles are altogether absent; Exclusively made up of longitudinal bar (I), and interbar channel subfacies (H_3) with infrequent occurrence of ripple laminated facies (K) and sheet sandstone subfacies (J_2); Transverse bar subfacies (L_2) is exclusively confined towards top; Common Onlapping/downlapping relationship within barforms and channelforms; Channelforms are occasionally overlain by ripple laminations and rarely by planar laminae; Texturally the constituent sandstone bodies are more mature (Figs. 7E, F). Compositionally they are subarkosic towards basal part and quartz arenitic towards top (Fig. 7G). Presence of partially or thoroughly altered, sub-rounded to rounded feldspar grains increases up the section (Figs. 7E, F).	Mid-channel longitudinal bars attest their origin within braided river channel (Miall, 1988; Samanta *et al*, 2016). Comparative textural maturity and absence of pebbles as well as basal scours on the erosional surfaces point towards steadier flow; Palaeogeography had presumably been further distal; Occurrences of transverse bars indicate further decrease in flow strength; Textural and mineralogical maturity of the constituent sandstone bodies further support longer transportation; Greater amount of altered feldspar grains suggests further increase in chemical weathering rate.

Table 6: Architectural elements within the studied fluvial interval of the Badami Group

Architectural element	Description	Interpretation
Downstream accretion element (DAE)	Composed of sandstone, with or without pebbles or granules, internally characterized by large cross strata confining smaller down-dip cross strata (Fig. 5B), flat base and convex-up top; Smaller cross strata and the larger cross strata orientated in the same direction (Fig. 5B); Facies I corresponds to this element.	Presence of DAE represents longitudinal bar; Repeated accretion of smaller ripples along the downstream side of the longitudinal bars presumably gave rise to this element (Miall, 1985, 1996; Long, 2011).
Lateral Accretion Element (LAE)	Composed of thin sheets of pebble-free sandstone internally characterized by tabular cross strata (Fig. 5F), rare in occurrence, always found to recline on the flanks of the DAEs or may overlie them; Cross strata orientations are at high angle to that of DAE and small channel element (SCE, described below; Fig. 5F); Subfacies L_1 corresponds to this element.	Accretion of the bars at high angle to the migration direction of DAE; Relationship with the DAE suggests bar-flank accretion; Sediments transported across the bar crest and avalanching down the flank of the longitudinal bar by secondary flows during low water stage (Long, 2011).
Small Channel Element (SCE)	Composed of lenticular sandstone bodies, may or may not be pebbly, internally characterized by cosets of trough cross strata (Figs. 4E, 4F, 5A); Cross set thickness as well as grain size decreases upward, In transverse section, base is generally concave-up, sometimes flat to slightly convex-up when overlying SGE (described below), while the top is flat; Mostly associated with DAE, often showing onlapping/ downlapping relationship; Maximum measured thickness up to 3.4 m, outcrop length along the direction of current is about 10s of m; This element corresponds to facies H.	The SCE represents the floor of the river channels or individual branches of braided rivers (Miall, 1985; Long, 2011); Upward decrease in grainsize along with reduction in cross set thickness clearly suggest decreasing flow strength with time (Bridge, 2006).
Laminated Sandsheet Element (LSE)	Characterized by sandstone, may or may not granule or pebble rich, tabular, sheet-like or wedge-like in geometry, averaging 25 cm thick and laterally traceable beyond 2 m; Planar lamina constitute the most common type of structure (Figs. 5C, D), although ripple lamina are also discernible (Fig. 5E); The former variety overlies both the DAE and SCE	LSE apparently formed at diverse locations with respect to river channels, such as, on top of bars or over small channel fills; Predominance of planar laminae supports high flow regime sheet flow, both on top of the bar, as well as, over the channelform during

	occasionally, the latter variety overlies the SCE only, though comparatively rare; Facies J and K correspond to this element.	low water stage; Ripple laminae formed during decrease in flow strength at final stage of channel filling.
Sediment Gravity-flow Element (SGE)	Sandy variety composed of very poorly sorted, coarse to medium grained sandstone with chaotically arranged oversized pebbles; Conglomeratic variety composed of matrix supported conglomerate with haphazard clast orientation; Lenticular with flat to concave-up bases and slightly convex-up tops (Figs. 3D, 4C); Internally massive, with rare crude cross stratifications; Maximum measured thickness 85 cm; Corresponds to facies B and subfacies G_1, commonly associated with SCE and DAE, comparatively with coarser associations.	Product of hyperconcentrated flow with high matrix strength, possibly generated during flash floods; Gradually become more fluidal with shedding of sediments, and consequently produce crude cross stratifications.
Transverse Bar Element (TBE)	Composed of poorly sorted medium to fine grained lenticular sandstone with flat bases and convex-up tops in transverse section (Fig. 6A); Internally tabular cross stratified, maximum thickness 56 cm (Fig. 6A), relatively rare, always overlies major erosion surfaces presumably channel floors; Cross strata orientation consistent with the associated SCE (Fig. 6A). Corresponds to subfacies L_2.	Tabular cross stratified sandstone bodies represent transverse bar (Yu *et al*., 2002). Directional similarities with cross strata in the SCE corroborates the contention (Sarkar *et al*., 2012).